Podoplanin expression in fibroblasts determines lymph node architecture and adaptive immune function

Spyridon Makris[1], Yukti Hari-Gupta[1], Jesús A. Cantoral-Rebordinos[1,2*], Victor G. Martinez[1,3*], Harry L. Horsnell[1], Charlotte M. de Winde[1,4*], Tanya Singh[5], Martina Jovancheva[1], Robin Kettler[5], Janos Kriston-Vizi[6], and Sophie E. Acton[1,✉]

[1]Stromal Immunology Group, MRC Laboratory for Molecular Cell Biology, University College London, Gower Street, London WC1E 6BT, UK
[2]Stem Cell and Human Development Laboratory, The Francis Crick Institute, 1 Midland Road, NW1 1AT
[3]Molecular Oncology Unit, Centro de Investigaciones Energéticas, Medioambientales y Tecnológicas (CIEMAT), Madrid, Spain
[4]Amsterdam UMC location Vrije Universiteit Amsterdam, Molecular Cell Biology and Immunology, De Boelelaan 1117, Amsterdam, the Netherlands
[5]Cell Signalling and Autophagy, MRC Laboratory for Molecular Cell Biology, University College London, Gower Street, London WC1E 6BT, UK.
[6]Bioinformatic group, Laboratory for Molecular Cell Biology, University College London, Gower Street, London WC1E 6BT, UK
[*]Current location

Lymph nodes are uniquely organised to form specialised niches for immune interactions. Fibroblastic reticular cells (FRCs) are an essential stromal component of lymph nodes – forming intricate 3-dimensional networks to facilitate communication between immune cells and depositing and ensheathing extracellular matrix on the conduit network. However, beyond these structural roles, FRCs regulate immune function through the production of growth factors, chemokines and inflammatory cues. Here we sought to determine how the immunoregulatory properties of FRCs are determined. Since PDPN has been implicated in lymph node development, we directly tested how the PDPN/CLEC-2 signalling axis impacted the immunoregulatory properties of FRCs *in vitro* and *in vivo*. We find that FRCs use the PDPN/CLEC-2 signalling axis to switch transcriptional states and alter the expression of immune related genes. *In vivo*, genetic deletion of PDPN from fibroblastic stroma in PDGFR$\alpha^{\text{mGFP}\triangle\text{PDPN}}$ mice downregulated key immunoregulatory molecules CCL21, VCAM-1 and ICAM-1 and attenuated the activation, proliferation and differentiation of lymphocyte populations. Further, PDGFR$\alpha^{\text{mGFP}\triangle\text{PDPN}}$ mice exhibited severe disruption of the FRC network structure, leading to a failure to separate B and T lymphocytes and misdistribution of myeloid cells through the tissue. We conclude that PDPN expression controls signalling pathways beyond cytoskeletal regulation and cell mechanics and that PDPN expression is required for FRC phenotype and function in lymph nodes.

Lymphoid tissue | Fibroblastic reticular cell | Podoplanin | Adaptive Immunity | Tissue biology

Correspondence: ***s.acton@ucl.ac.uk***

Introduction

Lymph nodes are key organs for immunity, providing the ideal meeting points for immune cells and coordinating the response to tissue damage and infection (1–3). Lymph nodes begin to develop at E12.5-E13.5 and are initially composed of both haematopoietic lymphoid tissue inducer (LTi) and stromal lymphoid tissue organiser cells (LTo) cells (2, 4, 5). The lymph node tissue supports the recruitment of immune cells but can also support their expansion during inflammation (1, 6, 7). Importantly, in order to accommodate rapidly rising cell numbers, lymph nodes need to reversibly expand (6). Lymph nodes achieve this by maintaining a highly organised compartmentalisation which is characterised by the cells in each area (8, 9). The most abundant cells in the lymph node are B and T lymphocytes. They are recruited to distinct areas of the follicular and parenchymal regions of the lymph node. B and T lymphocytes interact closely with their microenvironment which is composed of other immune as well as stromal cells (5). Stromal cells constitute a small fraction of the total cells in the lymph node however they are critical for supporting immune cells both during the steady state and disease. Much is now known about the construction of lymphoid tissues through development, and the signals required for commitment and differentiation of specialised lymphoid tissue stroma (10–12). However, we do not know how mature, adult lymphoid tissues maintain immunoregulatory properties through steady state and inflammatory contexts.

Fibroblastic reticular cells (FRCs) are the most abundant stromal cells of the lymph node forming an interconnected network which supports both the structural integrity of lymph nodes (13) and the various immune niches. Recent advances in scRNA-seq have shown high levels of heterogeneity of FRCs and their ability to specifically support distinct niches of immune cells (10, 14). FRCs express the chemokines CCL19 and CCL21 to facilitate the meeting of antigen-presenting dendritic cells and naïve T cells (14–16). FRCs proximal to high endothelial venules express high levels ICAM-1 and VCAM-1, important adhesion molecules, supporting the recruitment of both T and B lymphocytes from the circulation (17). FRCs proximal to B cell follicles are characterised by their high expression of CCL21 and BAFF-1 to support B cell survival (18–20). FRCs of lymph nodes are the archetype 'immunofibroblast' with the power to coordinate adaptive immune responses. As lymph nodes form in embryonic development, mesenchymal precursor cells expand and acquire specialized immunological features to attract and retain immune cells. It is not understood how such a ubiquitous cell type such as a fibroblast adapts to support immune functions. Here we aim to test how the immune reg-

ulatory capacity of FRCs is determined.

A common feature of all FRC subsets in the lymph node is their expression of podoplanin (PDPN). PDPN is a small transmembrane glycoprotein whose functions have been described in different contexts in both health and disease and is important in platelet aggregation, the separation of the lymphatic and endothelial vasculature, and in cell maturation and migration during development (21, 22). Podoplanin is expressed on several cell types including platelets, kidney podocytes (23), osteocytes (24), alveolar epithelial cells (25), keratinocytes (26), lymphatic endothelial cells (LECs) (2, 27, 28) and constitutively expressed in FRCs (29). Moreover, PDPN levels are upregulated in inflamed tissues (30), rheumatoid arthritis (31), in cancer cells and cancer-associated fibroblasts (32, 33) and during infection (34). PDPN was first described as a ligand for dendritic cell (DC) migration through the interaction with C-type lectin-like receptor CLEC-2 (6). Later it was shown that this same interaction promotes lymph node expansion through the regulation of FRC contractility and regulates the unilateral deposition of extracellular matrix into the conduit network (5–7, 35). Podoplanin maintains actomyosin contractility via activation of the cytoskeletal regulators ezrin and moesin (36), two members of the ERM (ezrin, radixin and moesin) family, which tether the cortical actin cytoskeleton to integral proteins in the plasma membrane (37). Most recently, we have described PDPN as a mechanical sensor in FRCs required to trigger FRC proliferation in response to increasing tissue tension through lymph node expansion (38). Mice with full knockout of PDPN fail to develop lymph nodes (39) and die shortly after birth due to circulatory defects (40, 41), however the function of PDPN has not been fully explored specifically in FRCs, or in adult lymphoid tissues. These findings suggest a more extensive role for PDPN in lymph node tissue function, beyond control of actomyosin contractility. We therefore undertook a detailed analysis of how the PDPN/CLEC-2 signalling axis determines transcriptional states in FRCs and tested these findings *in vivo*.

We utilised a combination of immortalised FRC lines and a mouse model (PDGFRα-mGFP-CreERT2) for conditional genetic manipulation of fibroblasts. Platelet derived growth factor alpha (PDGFRα) was chosen for its broad expression in mesenchymal cells and their progenitors. Further, PDGFRα has been identified as a universal fibroblast marker through extensive single cell transcriptomic analysis of fibroblasts across a range on tissues and inflammatory states (10). This model allows us to visualise the fibroblastic reticular network structure and to conditionally delete PDPN at desired timepoints in steady state or through an ongoing adaptive immune response. In this way we can now assess the function of podoplanin in adult lymphoid tissue function.

Results

PDPN/CLEC-2 signalling induces genome-wide changes in transcription by two independent modes of regulation. We first asked whether the PDPN/CLEC-2 axis regulates gene expression in FRCs. To test this, we silenced PDPN expression in FRC cell lines (PDPN KD), added recombinant CLEC-2 and subjected the cells to bulk RNA-sequencing (Fig. 1a). Bulk RNAseq provides a robust, reproducible readout of the average cell state which is the optimal approach for understanding the broad effects of PDPN/CLEC-2 signalling axis. We studied the effect of CLEC-2 after 0, 6 and 24 hours, to compare immediate, direct transcriptional changes and long-term indirect changes to the FRC transcriptome. We used a stringent limit for differentially expressed genes, setting cut-off values at fold change ± 1.6 and adjusted p-values at <0.05. We observed that PDPN KD had significant effects on gene expression resulting in downregulation of 1033 genes (categorised as PDPN-driven) and upregulation of 593 genes (categorised as PDPN-downregulated) (Fig. 1b) (Supplementary table 1). When we studied the genes transcriptionally regulated after treatment with CLEC-2 for 6 hours, we found 794 CLEC-2 upregulated genes and 1119 CLEC-2 downregulated genes (Fig. 1c). Interestingly, we observed fewer differentially expressed genes after treating the cells with CLEC-2 for 24 hours than for 6 hours (351 downregulated genes and 187 upregulated) (Fig. 1d). This finding supports previous knowledge that CLEC-2 signalling is transient in FRCs (35) and points to a transient transcriptional regulation of CLEC-2, with the majority of CLEC-2 regulated genes returning to basal levels *in vitro* after 24 hours.

It has been previously reported that signalling of PDPN to cytoskeletal modulators is dampened by binding of CLEC-2 and exposing FRCs to CLEC-2 phenocopies a loss of PDPN in the context of actomyosin contractility (6). Therefore, we asked whether CLEC-2 upregulated genes correlated with PDPN KD. We expected significant overlap in the gene signatures since CLEC-2 is the only known binding partner of PDPN in the context of FRC biology. We found some overlap between the genes regulated by PDPN or CLEC-2 (Fig. S1). However, we found that this was only the case for a small fraction of genes (85 and 236 genes), and several genes displayed the opposite behaviour (109 and 92 genes). We next sought to identify the genes regulated by PDPN in the steady-state independently of CLEC-2 (Fig. 1e). We found 84 PDPN-dependent genes whose expression did not change in the presence of CLEC-2 at either 6 or 24 hours (Fig. 1e) indicating that PDPN drives a transcriptional programme in FRCs independent of ligand binding. The PDPN-dependent upregulated genes included fibroblast markers (*Thy1*), vesicular transport and autophagy (*Atg3*, *Atg12*, *Pink1*, *Lamp2*, *Dnm1*, *Tapb2*), cell signalling (*Jak2*, *Gatsl3*, *Dusp16*), actin dynamics (*Rnd1*, *Ssh3*), and cell communication genes (*Cxcl12*, *Ptgs1*, *Efnb2*, *Efna2*, *Olfml3*, *Fzd7*, *Bdnf*) and transcription factors (*Sox11*, *Ahr*, *Hoxd9*, *Cxxc5*) (Fig. 1e).

We next asked which genes were regulated by CLEC-2 specifically through binding PDPN (Fig. 1f). Hierarchical clustering revealed four PDPN and CLEC-2 dependent groups. The two largest clusters were downregulated by CLEC-2 at 6 hours (including the Wnt ligands *Wnt4* and *Wnt7b*, and the extracellular matrix components *Tnn* and

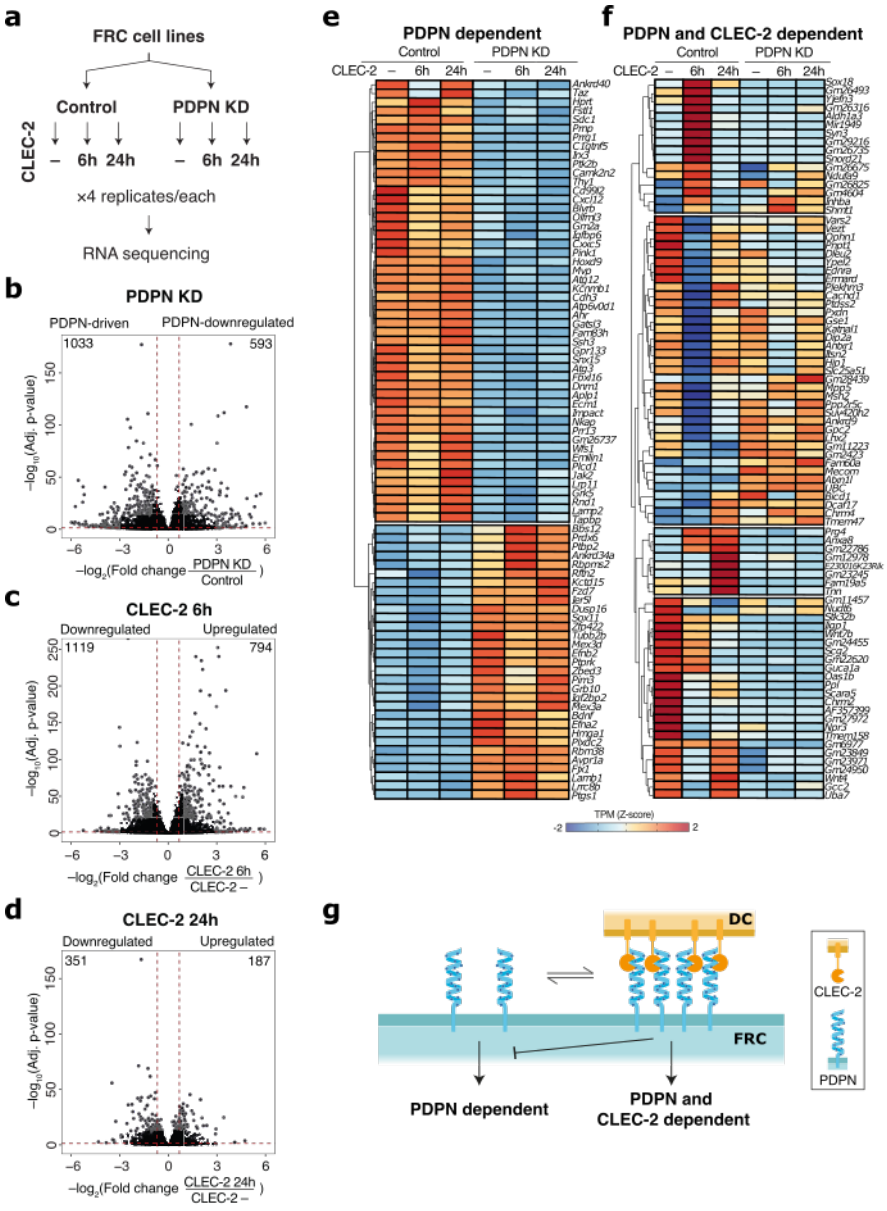

Fig. 1. The PDPN/CLEC-2 signalling axis controls the transcriptional landscape of cultured fibroblastic reticular cells a, Schematic of the experimental setup. FRC cell lines expressing basal levels of PDPN (Control) or expressing a silencing RNA for podoplanin (PDPN KD) were cultured for 0, 6 or 24 hours with CLEC-2 and subjected to RNA-sequencing (4 replicates per condition). **b,** Volcano plot showing changes in gene expression after PDPN-KD (compared to Control, no CLEC-2). Differentially expressed genes were categorised into PDPN-driven and PDPN-downregulated genes based on fold change and adjusted p-values. **c,d,** Volcano plot showing changes in gene expression after culture with CLEC-2 **c,** 6 hours or **d,** 24 hours (compared to Control, no CLEC-2). Differentially expressed genes were categorised into CLEC-upregulated and CLEC-downregulated genes based on fold change and adjusted p-values. **e,** Heatmap of the genes regulated by PDPN expression irrespective of CLEC-2 signalling. **f,** Heatmap of the genes regulated by CLEC-2 only when PDPN is expressed. **g,** Diagram of the modes of transcriptional regulation, one maintained by podoplanin expression only (PDPN dependent) and an alternative maintained by PDPN and CLEC-2 (PDPN and CLEC-2 dependent).

Prg4). Moreover, most genes in this group suggested that CLEC-2 stimulation drives an independent transcriptional profile distinct from PDPN alone. Indeed, only a small fraction of these genes followed the previously reported pattern phenocopying PDPN KD. We therefore propose that there are two distinct modes of transcriptional regulation, one which is PDPN-dependent in steady state and one which is PDPN and CLEC-2 dependent (Fig. 1g). We next sought to investigate which cellular functions are regulated by the PDPN/CLEC-2 axis.

Gene ontology analysis of the genes regulated by PDPN/CLEC-2 transcriptional targets. We asked which cellular processes are regulated by PDPN expression in steady state versus CLEC-2 stimulation of PDPN in FRCs. We performed gene-enrichment analysis using the GO Biological Process (http://genontology.org) database to infer the cellular functions regulated by the differentially expressed genes. We found that PDPN-driven pathways included response to mechanical stimuli and extracellular matrix organisation as have been previously reported (35, 38) (Fig. 2a). Additionally, many terms were related to immune-related processes, including response to interferon (IFN)-β and IFN-γ, response to viral replication and inflammation. This suggests that PDPN drives gene expression relevant to immune-regulatory FRC functions in the absence of CLEC-2 (Fig. 2a). The most over-represented pathways downregulated by PDPN included non-lymphoid tissue functions such as epithelium morphogenesis, lung development, odontogenesis or axon guidance (Fig. 2b). Signalling pathways, JNK cascade ERK1/2 and steroid hormone signalling were also suppressed by PDPN expression in steady state (Fig. 2b).

The processes regulated by CLEC-2 included positive regulation of collagen biosynthesis as have been previously reported (35). In addition, CLEC-2 drove a positive regulation of cell differentiation and cell division (Fig. 2c). CLEC-

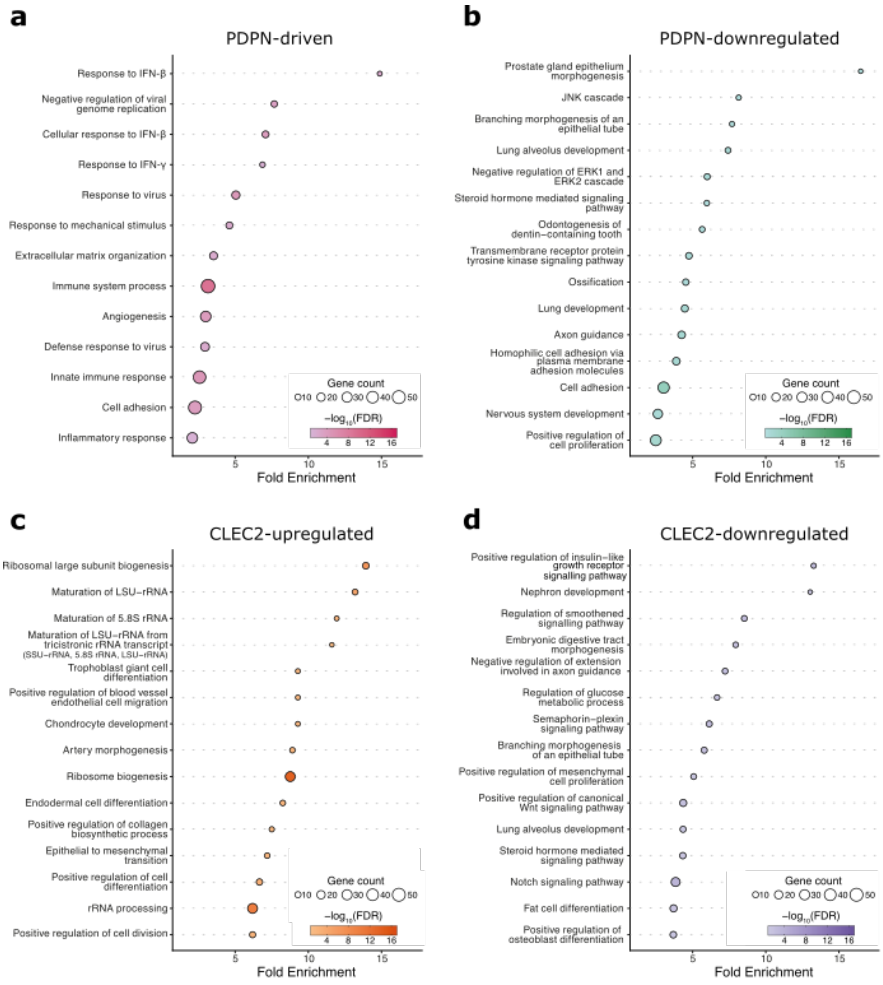

Fig. 2. Functional annotation of the PDPN/CLEC-2 differentially expressed genes Gene enrichment analysis using the Biological Process GO Terms database on DAVID. The top 15 GO terms ranked by fold enrichment (observed/ expected genes per term) and filtered by adjusted p-value (p.adj < 0.05) are shown for **a,** PDPN driven **b,** PDPN downregulated **c,** CLEC-2 upregulated **d,** and CLEC-2 downregulated genes. Dot colour represents statistical significance ($\log_2$ FDR) and size is proportional to gene count (number of genes annotated in each GO term).

2 downregulated genes mapped to signalling processes, including the insulin growth factor receptor (*Igfr*), smoothened, semaphoring-plexin, *Wnt*, *Notch* and steroid signalling pathways, (Fig. 2d). Strikingly, the most overrepresented GO terms for CLEC-2 upregulated genes were related to translation, ribosome biogenesis and ribosomal RNA transcription and processing, suggesting an extensive change in cell state and function.

PDPN–CLEC-2 signalling transcriptionally regulates extensive functional networks. The wide range of cellular functions identified by GO mapping prompted us to study how these differentially expressed genes could act in a coordinated manner in FRCs. We used the STRING functional annotation platform to study functional networks, including physical interactions as well as functional connections. We then clustered the genes based on their interactions. PDPN-driven genes formed a large cluster of immune-related genes (Fig. 3a and Supplementary table 2). This cluster included membrane receptors (*Cd47*, *Itgb2*), cytokine signalling (*Stat1*, *Stat2*, *Irf7*, *Fit1*, *Ifit1*, *Ifit3*, *Cxcl1*, *Cxcl10*, *Cxcl5*, *Ccl2*, *Ccl9*), several collagen genes, ECM components (*Ecm1*, *Timp3*) consistent with early microarray analysis of lymph node stromal cells (42), complement genes (*C2*, *C3*, *C1ra*, *C1s1*, *C1s2*), and genes related to antigen presentation (*Anpep*, *H2-T23*, *H2-K1*). While the well-described function of PDPN is actomyosin contractility, our data suggests that signalling through the PDPN/CLEC-2 axis is also relevant for maintaining an immune-specific fibroblast phenotype.

PDPN downregulated genes (Fig. 3b and Supplementary table 2) formed dispersed clusters with functions that were unrelated to fibroblasts or lymph node biology, including neuronal receptors and signalling proteins (*Adora2*, *Mc4r*, *Ptger4*, *Gria2*, *Gria4*, *Shank2*, *Efna2*, *Efnb2*, *Epha3*), and axon guidance (*Adamts6*, *Adamts14*, *Spon1*, *Sema5a*). The remaining clusters were associated with signalling modules, extracellular matrix components (*Tnc*, *Itga6*, *Itga6*, *Lama2*, *Lama5*, *Col11a1*, *Col19a1*, *Tll1*, *Play*, *Cd33*) and secreted factors (*Bdnf*, *Bmp4*, *Fgf10*, *Fgf22*). These data suggest that PDPN may act to control specificity of the extracellular matrix that is secreted by FRCs.

CLEC-2 upregulated genes formed a large cluster of hits related to ribosome biogenesis and regulation of translation (Fig. 3c and Supplementary table 2). Moreover, in line with the PDPN-driven genes, we found a wealth of clusters related to immune-related functions and signalling, including different families of growth factors (*Tgfb*, *Vegf*, *Pdgf*), genes involved in inflammation, wound healing, and an-

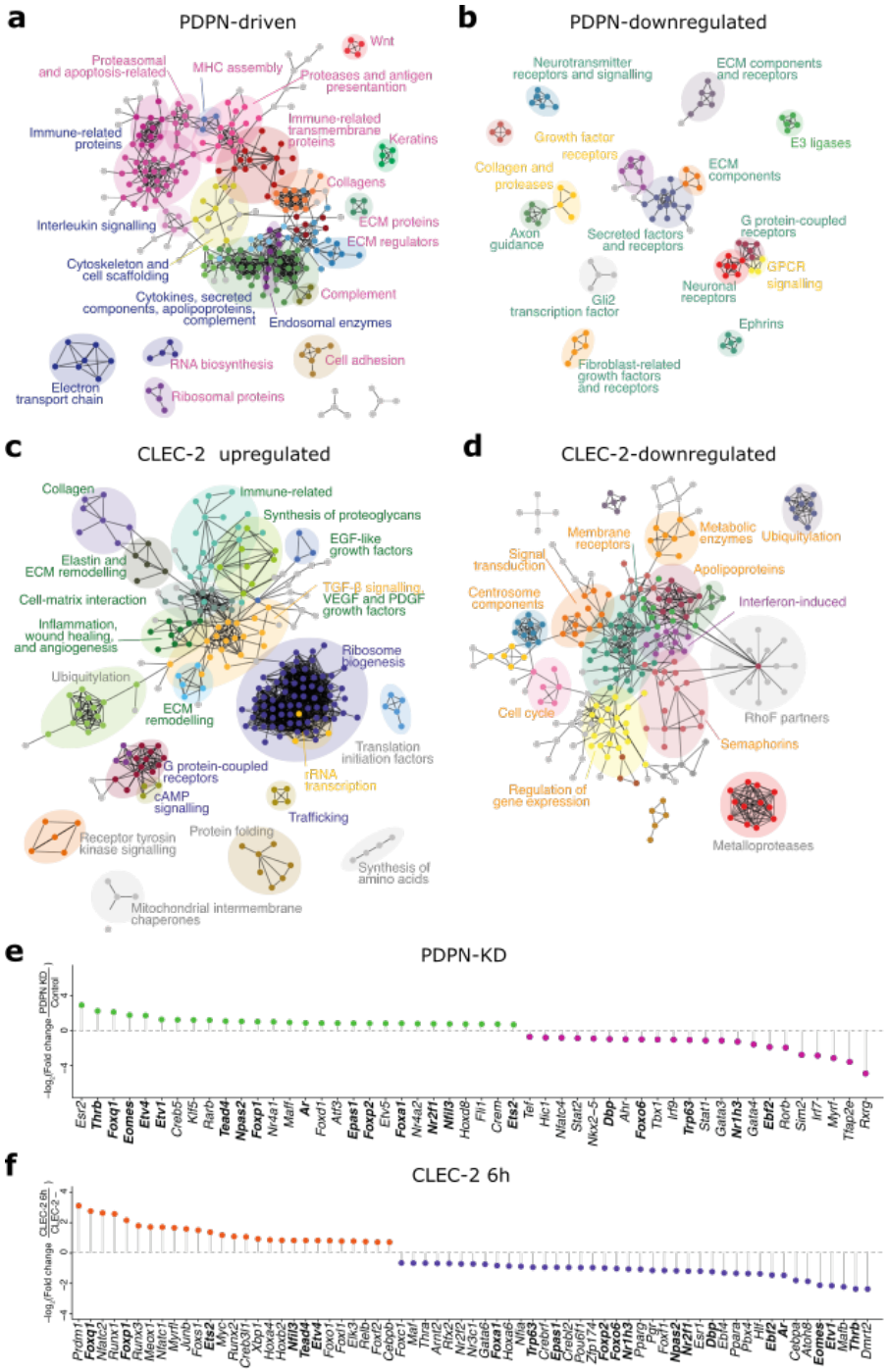

Fig. 3. PDPN/CLEC-2 transcriptional targets form extensive functional networks Functional annotation of PDPN/CLEC-2 differentially expressed genes showing **a,** PDPN-driven, **b,** PDPN-downregulated, **c,** CLEC-2 upregulated and **d,** CLEC-2 downregulated genes. The differentially expressed gene lists were analysed in the STRING functional annotation platform. Nodes not forming part of a larger network were hidden (fewer than 3 neighbours at level 3) and the remaining genes were clustered using MCODE. Clusters were manually annotated based on gene description. Expression values (log2 Fold change) of the transcription factors regulated by **e,** PDPN-KD or treatment with **f,** CLEC-2 for 6 hours.

giogenesis. Interestingly, other clusters included translation initiation factors, trafficking, protein folding, synthesis of amino acids and mitochondrial intermembrane chaperones. CLEC-2 downregulated genes were related to signalling, metabolism, apolipoproteins, regulation of gene expression, cell cycle and cell division (centrosome components) as well as metalloproteases (including several members of the *Adamts* family) (Fig. 3d Supplementary table 2).

Our data now shows that the PDPN/CLEC-2 signalling axis can drive extensive transcriptional programmes. We next asked which transcription factors were themselves transcriptionally regulated by the PDPN/CLEC-2 axis (Fig. 3e,f). Of note, the PDPN/CLEC-2 axis regulated expression levels of *Tead4* and *Lef1*, transcription factors that interact with the Hippo pathway effectors YAP and TAZ (Fig. 3e,f). YAP/TAZ signalling has been reported to direct the commitment of FRCs in lymph nodes (11). In our RNAseq data we find that PDPN and CLEC-2 transcriptionally regulate the Hippo pathways at many levels, ligand expression, effector proteins, transcription factors and target genes (Fig. S2). Therefore, we hypothesised that PDPN/CLEC-2 signalling could also determine FRC phenotype and function through regulation of the Hippo pathways in homeostatic adult tissues. The large number of genes transcriptionally regulated by PDPN/CLEC-

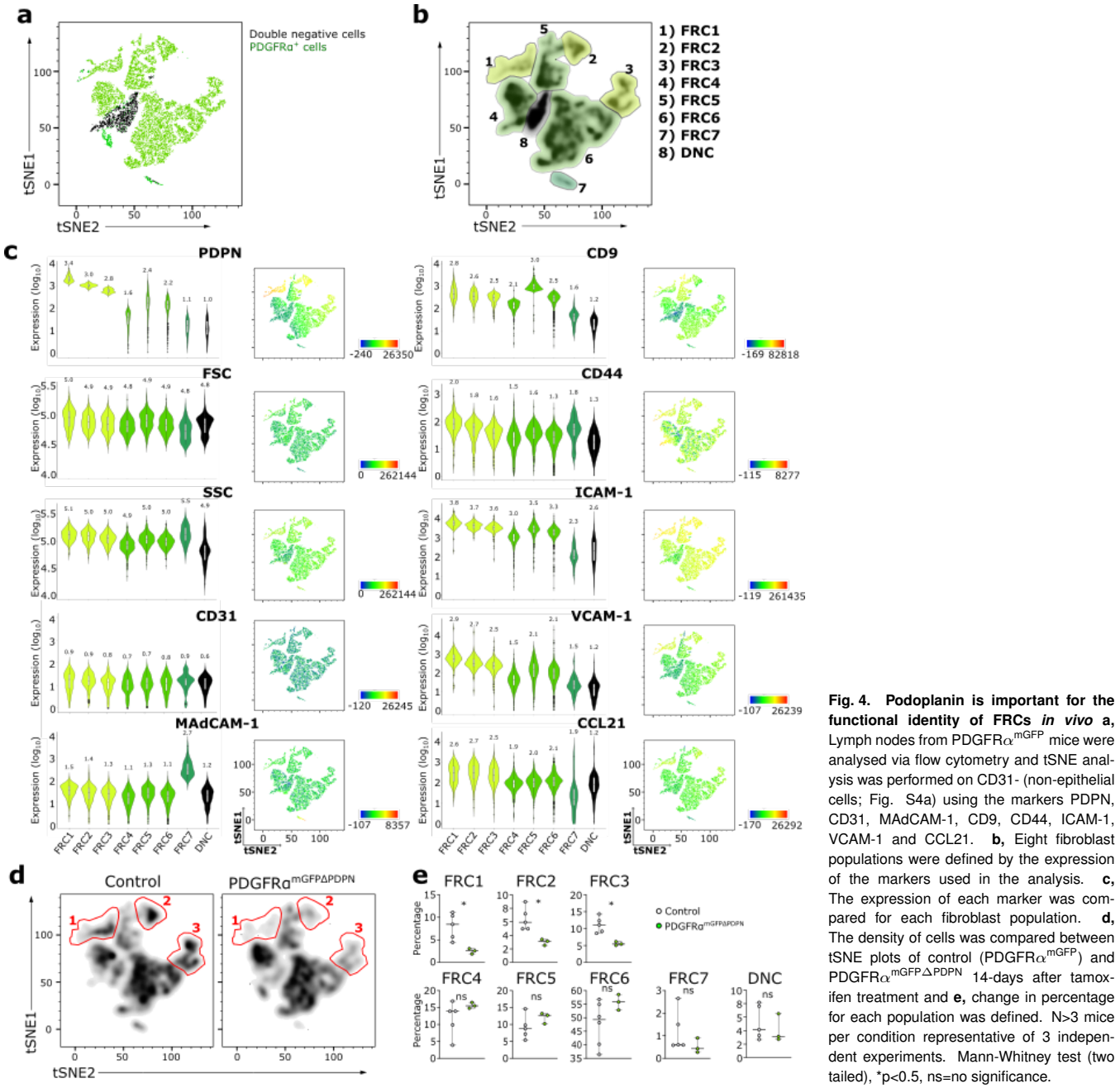

Fig. 4. Podoplanin is important for the functional identity of FRCs *in vivo* a, Lymph nodes from PDGFRα^{mGFP} mice were analysed via flow cytometry and tSNE analysis was performed on CD31- (non-epithelial cells; Fig. S4a) using the markers PDPN, CD31, MAdCAM-1, CD9, CD44, ICAM-1, VCAM-1 and CCL21. **b,** Eight fibroblast populations were defined by the expression of the markers used in the analysis. **c,** The expression of each marker was compared for each fibroblast population. **d,** The density of cells was compared between tSNE plots of control (PDGFRα^{mGFP}) and PDGFR$\alpha^{mGFP\Delta PDPN}$ 14-days after tamoxifen treatment and **e,** change in percentage for each population was defined. N>3 mice per condition representative of 3 independent experiments. Mann-Whitney test (two tailed), *p<0.5, ns=no significance.

2 could amplify signalling and act as positive feedback loops to determine and reinforce specific programmes that dictate FRC identity.

Podoplanin drives the functional profile of FRCs *in vivo*. To test our hypothesis that PDPN signalling impacted FRC phenotype and function we developed a knock-in mouse model (PDGFRα-mGFP-CreERT2) to track and conditionally genetically manipulate FRCs (Fig. S3a). We generated PDGFRα-mGFP-CreERT2 x PDPN$^{fl/fl}$ mice to delete PDPN specifically in PDGFRα fibroblastic stroma upon tamoxifen treatment (PDGFR$\alpha^{mGFP\Delta PDPN}$). We performed in-depth analysis of the FRC phenotypes using known surface markers driving key FRC functions in lymph nodes. We gated non-endothelial stromal cells (CD45$^-$CD31$^-$) (Figure S4a) and performed t-distributed stochastic neighbour embedding (tSNE) analysis using the functional markers (PDPN, CD31, MAdCAM-1, CD9, CD44, ICAM-1, VCAM-1 and CCL21). We could clearly identify a population of non-endothelial/non-epithelial stroma which were also negative for GFP (PDGFRα) (Fig. 4a). These 'double negative cells' (DNC) have been identified previously as a pericyte population, but their phenotype and function remain unclear (Fig. 4a) (42, 43). We defined 8 fibroblastic stromal populations within the tSNE analysis and identified high expression of MAdCAM-1 on FRC7 suggesting these might be the marginal zone reticular subset (MRC) (Fig 4a-c). We could not isolate enough follicular dendritic cells (FDC) in this analysis, so we focus on FRC populations. The FRC populations had varied expression of PDPN, where FRC1-3

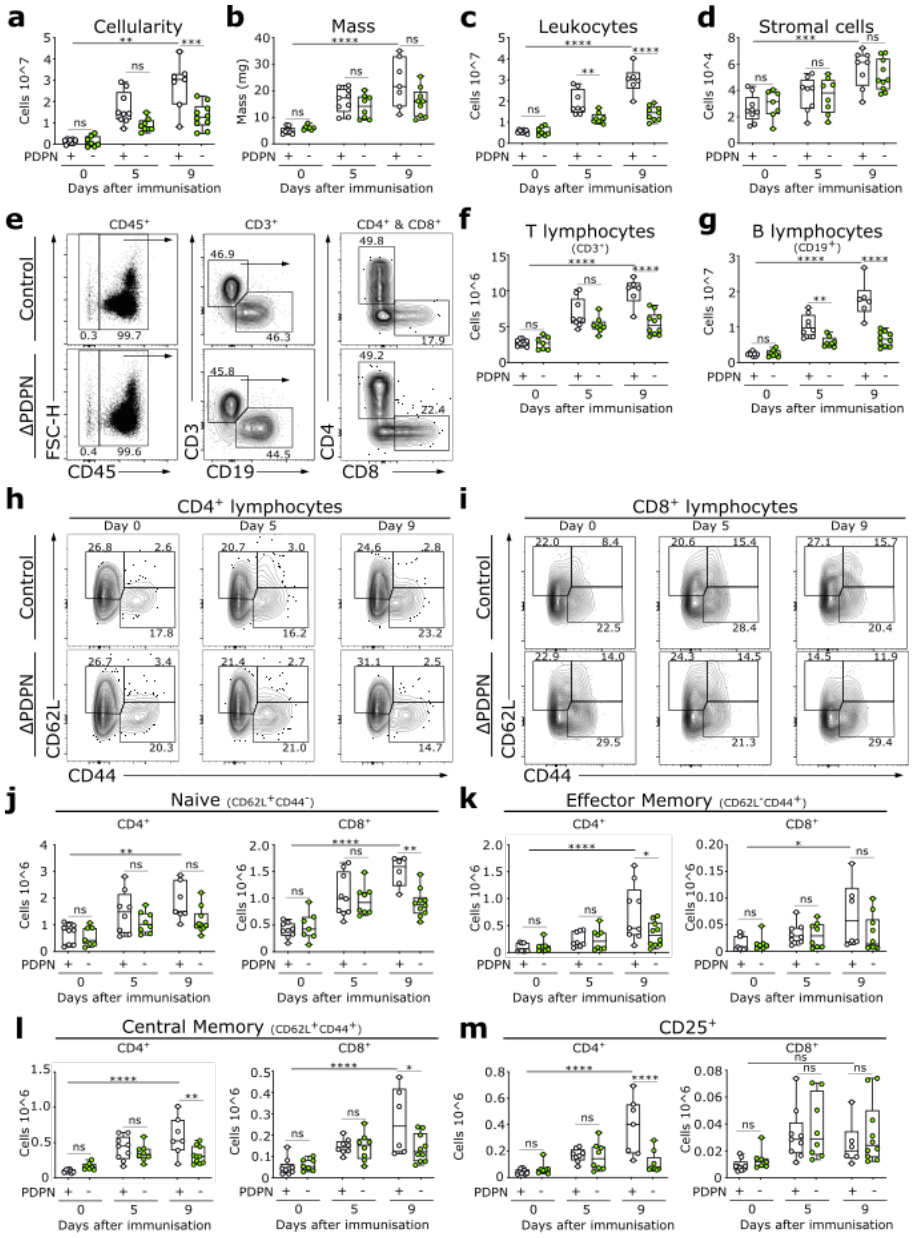

Fig. 5. Lymph node expansion following immunisation is attenuated in PDGFR$\alpha^{mGFP\Delta PDPN}$ mice. PDGFRα^{mGFP} (open circle) or PDGFR$\alpha^{mGFP\Delta PDPN}$ (green circle) mice were immunised subcutaneously with Incomplete Freund's Adjuvant (IFA) or Complete Freund's Adjuvant (CFA) and ovalbumin 7 days after tamoxifen treatment. **a,** Total cell number, **b,** mass, **c,** leukocytes and **d,** stromal cells were analysed for each lymph node. **e,** Gating strategy used to quantify the subsets of **f,** T lymphocytes and **g,** B lymphocytes. T lymphocytes further gated to examine the activation of **h,i,** $CD4^+$ or $CD8^+$ cells and **j,** Naïve ($CD62L^+CD44^-$), **k,** effector memory ($CD62L^-CD44^+$), **l,** central memory cells ($CD62L^+CD44^+$) and **m,** $CD25^+$ T lymphocytes were quantified. N>6 mice, representative of 2 independent experiments. Two-way ANOVA, ****p<0.0001, **p<0.01, *p<0.05, ns=no significance.

were $PDPN^{hi}$ and FRC4-6 were $PDPN^{int}$ (Fig. 4c). ICAM-1, VCAM-1 and CCL21, are key molecules controlling the migration of T cells within lymph nodes (14, 15, 44) and were highest expressed in the $PDPN^{hi}$ populations (FRC1-3) (Fig. 4c). The PDPN binding partner CD9, a tetraspanin which regulates FRC-FRC interactions in vitro was highest expressed in FRC5 (45). We could now examine which FRC populations are most affected by PDPN deletion *in vivo*. The density plot analysis showed a significant reduction specifically in the $PDPN^{hi}$ populations FRC1-3 (Fig. 4d,e). The percentage of DNCs was unaffected suggesting that $PDPN^{del}$ FRCs are still phenotypically distinct from DNCs (Fig. 4e). These data support that expression of PDPN does indeed affect the phenotype and identity of FRCs in fully developed adult lymph nodes.

T cell activation is attenuated *in vivo* in PDGFR$\alpha^{mGFP\Delta PDPN}$ mice. Our *in vivo* data suggest deletion of PDPN from FRCs may affect immune cell recruitment, migration, or activation due to the consequent reduction of ICAM-1, VCAM-1 and CCL21 expression on FRCs. We next examined if the deletion of PDPN alters adaptive immune responses *in vivo* after immunisation. The lymph node cellularity, mass, leukocyte ($CD45^+$) and stromal cell populations ($CD45^-$) were similar in steady state between control and PDGFR$\alpha^{mGFP\Delta PDPN}$ mice but attenuated after immunisation (Fig. 5a-d; gating on Fig. S4b and Fig. S5). LEC and blood endothelial cell (BEC) populations expanded independently of PDPN deletion in FRCs however the number of FRCs was specifically reduced in the PDGFR$\alpha^{mGFP\Delta PDPN}$ lymph nodes at day 9 post-immunisation (Fig. S6a). We have shown previously that PDPN is a mechanical sensor in FRCs and is required to

trigger FRC proliferation in response to increased mechanical strain as the lymph node begins to expand (38) which can explain the reduction in FRC numbers. The number of B and T lymphocytes was unchanged in PDGFR$\alpha^{mGFP\Delta PDPN}$ mice in steady state, but all subsets were reduced in number post immunisation (Fig. 5e-g; Fig. S6b). We compared activation ($CD25^+$) and differentiation of $CD4^+$ and $CD8^+$ T cells and found reduced numbers of both central and effector memory T cell subsets (Fig. 5h-m; Fig. S5). There was also a significant reduction in the number of $CD4^+CD25^+$ T cells at day 9 (Fig. 5m; Fig. S5). These data suggest that the initial trapping of naïve lymphocytes is unaffected by PDPN deletion, but T cell activation and proliferation is constrained in PDGFR$\alpha^{mGFP\Delta PDPN}$ mice. Overall, these data show that PDPN deletion in FRCs does not affect recruitment of immune cells into the lymph node. However, lymphocyte activation is attenuated, leading us to hypothesise that antigen-presentation to T lymphocytes is impacted by PDPN deletion in FRCs.

Podoplanin regulates CCL21 availability and positioning of antigen-presenting cells. Podoplanin is known to be a ligand for CLEC-2 and to promote DC migration (6, 7). Our data now also show that PDPN deletion in FRCs reduces the expression of CCL21 by these stromal cells *in vivo* (Fig. 4). Both of these PDPN functions could disrupt DC migration and could explain reduced T cell activation and attenuated lymph node expansion following immune challenge (6). We therefore quantified and compared the number of both resident and migratory DCs in lymph nodes from control and PDGFR$\alpha^{mGFP\Delta PDPN}$ mice. We observed a clear reduction in the number of resident (40% reduction) and migratory DCs (30% reduction) present in the lymph node of PDGFR$\alpha^{mGFP\Delta PDPN}$ mice post-immunisation (Fig. 6a), suggesting that recruitment of migratory antigen-presenting cells to lymph nodes is inhibited in PDGFR$\alpha^{mGFP\Delta PDPN}$ mice. Further, tissue analysis of steady state lymph nodes showed that the location of MHC class II^{hi} cells, which we assume to be antigen-presenting leukocytes, in PDGFR$\alpha^{mGFP\Delta PDPN}$ mice was altered compared to controls (Fig. 6b). We observed areas of lymph node tissue almost devoid of MHC class II^{hi} cells, and other areas where MHC class II^{hi} cells were clustered in PDGFR$\alpha^{mGFP\Delta PDPN}$ mice, whereas in controls MHC class II^{hi} cells were evenly dispersed through the tissue. We quantified and correlated the expression of mGFP, PDPN and CCL21 in tissue sections to ask if spatial disruption of MHC class II^{hi} cells could be due to alterations to CCL21 availability in the FRC network (Fig. 6c-g). Quantifications of PDPN fluorescence intensity in tissue sections showed an approximate 35% reduction across the tissue regions analysed (Fig. 6c). In the same matched tissue regions, we also observed a reduction in CCL21 intensity (Fig. 6d). CCL21 expression correlated with the expression of mGFP indicating fibroblastic stroma are the source of CCL21 in the lymph node (Fig. 6e). Further we found that CCL21 correlated with PDPN expression, and therefore in PDGFR$\alpha^{mGFP\Delta PDPN}$ mice CCL21 was expressed at lower levels (Fig. 6f). We correlated PDPN and mGFP in control and PDGFR$\alpha^{mGFP\Delta PDPN}$ tissues (Fig. 6g) and found that lowest PDPN correlated with lower mGFP suggesting areas of the paracortex devoid of FRCs. We observe CCL21 is expressed on the $mGFP^+$ FRC network in PDGFRα^{mGFP} mice and is colocalised with PDPN (Fig. 6h). In PDGFR$\alpha^{mGFP\Delta PDPN}$ mice CCL21 is still observed on some mGFP cells but now we observe many $mGFP^+$ FRCs lacking both CCL21 and PDPN expression (Fig. 6h). These data suggest that deletion of PDPN in FRCs changes the stromal microenvironment and impacts recruitment and trafficking of antigen-presenting cells.

Podoplanin deletion disrupts FRC network integrity and stromal cell density. In additional to the mispositioning of antigen-presenting cells previously described, we also found that the FRC network was absent in many areas of lymph nodes from PDGFR$\alpha^{mGFP\Delta PDPN}$ mice (Fig. 6b,h). We therefore investigated the requirement for PDPN expression in FRCs for reticular network structure and lymph node tissue organisation in steady state. Tamoxifen treatment of PDGFR$\alpha^{mGFP\Delta PDPN}$ led to the reduced expression of PDPN specifically in FRCs but not LECs (Fig. 7a,b; Extended Data Fig. 4b-d).

We observed disrupted areas of the FRC network in various regions of the lymph nodes in PDGFR$\alpha^{mGFP\Delta PDPN}$ mice while the lymphatic vessels in the subcapsular sinus retained their structure and PDPN expression (Fig. 7c,d). The distribution of blood vessels (observed by perlecan staining) appeared altered and we observed more prominent basement membrane structures around vessels in in PDGFR$\alpha^{mGFP\Delta PDPN}$ mice (Fig. 7c,d). We observed areas of the paracortex tightly packed with leukocytes (nuclei stained with DAPI) but devoid of FRCs (identified by mGFP) (Fig. 7c,d). These tissue areas also lacked the extracellular matrix components of the conduit network suggesting that the reticular network had lost integrity (Fig. 7c,d). To quantify the disruption of the FRC network in the paracortex we used an ImageJ tool (Mitochondrial Network Analysis - MiNA) based on skeletisation to quantify mathematical properties of the network (Fig. 7e) (46). We find in PDGFR$\alpha^{mGFP\Delta PDPN}$ mice there is a 60% decrease in the number of branches, shortened branch length and a 25% decrease in the network footprint, confirming a severe disruption to the FRC network (Fig. 7f). Strikingly, we also observed that the B cell follicles were severely disrupted after PDPN deletion (Fig. 7g). The B cell areas were easily distinguished in control (PDGFRα^{mGFP}) mice by the expression of B220 and lack of CD3 (Fig. 7g). However, lymph nodes of PDGFR$\alpha^{mGFP\Delta PDPN}$ mice had lost the boundaries between the B cell follicles and the T cell areas. B cells were no longer clustered into distinct follicles in PDGFR$\alpha^{mGFP\Delta PDPN}$ mice but were now diffusely located deeper into the paracortex. We also observed that the disorganised B cell areas at the lymph node periphery in PDGFR$\alpha^{mGFP\Delta PDPN}$ mice have increased fibroblast ($mGFP^+$) density compared to controls (Fig. 7g(i-ii)). In control lymph nodes, B cell follicles are supported by a stromal network of FDCs which are a distinct form of FRCs and specifically support B cells through the production of

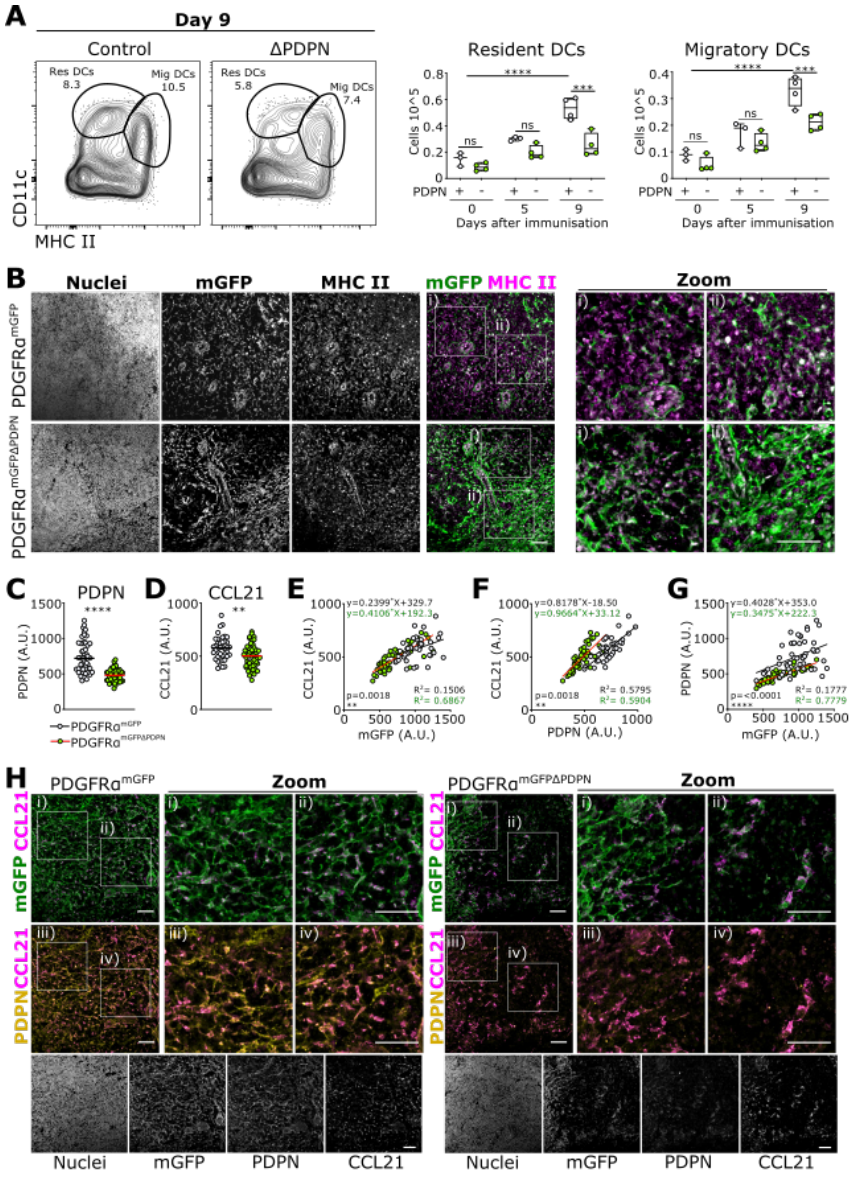

Fig. 6. Conditional deletion of podoplanin in FRCs disrupts tissue architecture a, Mice were tamoxifen treated and 7 days later immunisation with Complete Freund's Adjuvant before being harvested at days 5 and 9 post-immunisation or **b-h,** harvested 14 days after tamoxifen treatment alone. **a,** Flow cytometry plot gating on resident (Res DCs) and migratory (Mig DCs) dendritic cells 9 days following immunisation and number of resident and migratory DCs calculated by flow cytometry showing PDGFRα^{mGFP} (open circle) and PDGFR$\alpha^{mGFP\Delta PDPN}$ (green circle) cells. N=3-4 mice for each condition representative of 2 independent experiments. Mann-Whitney test (two tailed), ****p<0.0001, ns=no significance. Representative images of sections stained for: **b,** Nuclei (DAPI), mGFP and MHC class II staining and merged mGFP (green) and MHC class II (magenta) with (i-ii) representative zoom images comparing PDGFRα^{mGFP} and PDGFR$\alpha^{mGFP\Delta PDPN}$ lymph nodes. Scale bars 50 mum. N>3 mice per condition representative of 2 independent experiments. Expression of **c,** PDPN and **d,** CCL21 and correlation of **e,** mGFP vs CCL21, **f,** PDPN vs CCL21 and **g,** mGFP vs. PDPN. **c-g,** Quantified from 10 randomised selection from 5 images of the lymph node parenchyma. **c-g,** Comparison of PDGFRα^{mGFP} and PDGFR$\alpha^{mGFP\Delta PDPN}$ (ΔPDPN) using Mann-Whitney test (two tailed), ****p<0.0001, **p<0.01. **e-g,** linear regression analysis of each condition showing slope equation and R2. **h,** Representative images of FRC network stained for CCL21 (magenta), mGFP (green) or PDPN (yellow); and single channels staining for nuclei (DAPI), mGFP, PDPN and CCL21 in PDGFRα^{mGFP} and PDGFR$\alpha^{mGFP\Delta PDPN}$ parenchymal regions. (i-ii) Images of merged mGFP and CCL21; (iii-iv) or PDPN and CCL21. Scale bars 50 mum. N>3 mice per condition representative of 2 independent experiments.

CXCL13 for their recruitment, and growth factors such as BAFF (14, 18). FDCs also form the stromal scaffolds for germinal centre formation and retain and present antigen to B cells to support B cell selection (47). Since FDCs are also of mesenchymal origin and express PDGFRα (14) they are also conditionally targeted in our PDGFR$\alpha^{mGFP\Delta PDPN}$ mice. FDCs also express PDPN, although at lower levels than FRCs, but the function of PDPN in FDCs has not previously been investigated. Our data now suggest that PDPN could also play a critical role in FDC specification and function.

Overall, these *in vivo* data show a novel role of PDPN beyond the control of actomyosin contractility during immune responses as predicted by our *in vitro* transcriptional analysis. We show that PDPN can direct the immunoregulatory phenotype of fibroblastic stroma in lymph nodes and that genetic deletion of PDPN in adult tissues severely disrupts lymph node stromal architecture.

Discussion

We set out to investigate key signalling pathways required for the maintenance of lymph node function. Lymph node tissue architecture can lose integrity and function due to disease, ageing or pollution (48, 49). Understanding maintenance of lymphoid tissue function is therefore important for interpreting variability in immune responses throughout human lifetime (5). We focused on a key stromal structure, the fibroblastic reticular network, and since PDPN has been implicated in lymph node development, we directly tested how the PDPN/CLEC-2 signalling axis impacted the immunoregulatory properties of FRCs *in vitro* and *in vivo*. Our investigations have revealed that PDPN expression in fibroblastic stroma impacts adaptive immune function and regulates lymph node architecture and compartmentalization, dramatically disrupting antigen presenting cell, T cell and B cell localization in lymph nodes. We determine that PDPN drives two distinct transcriptional programmes which drive exten-

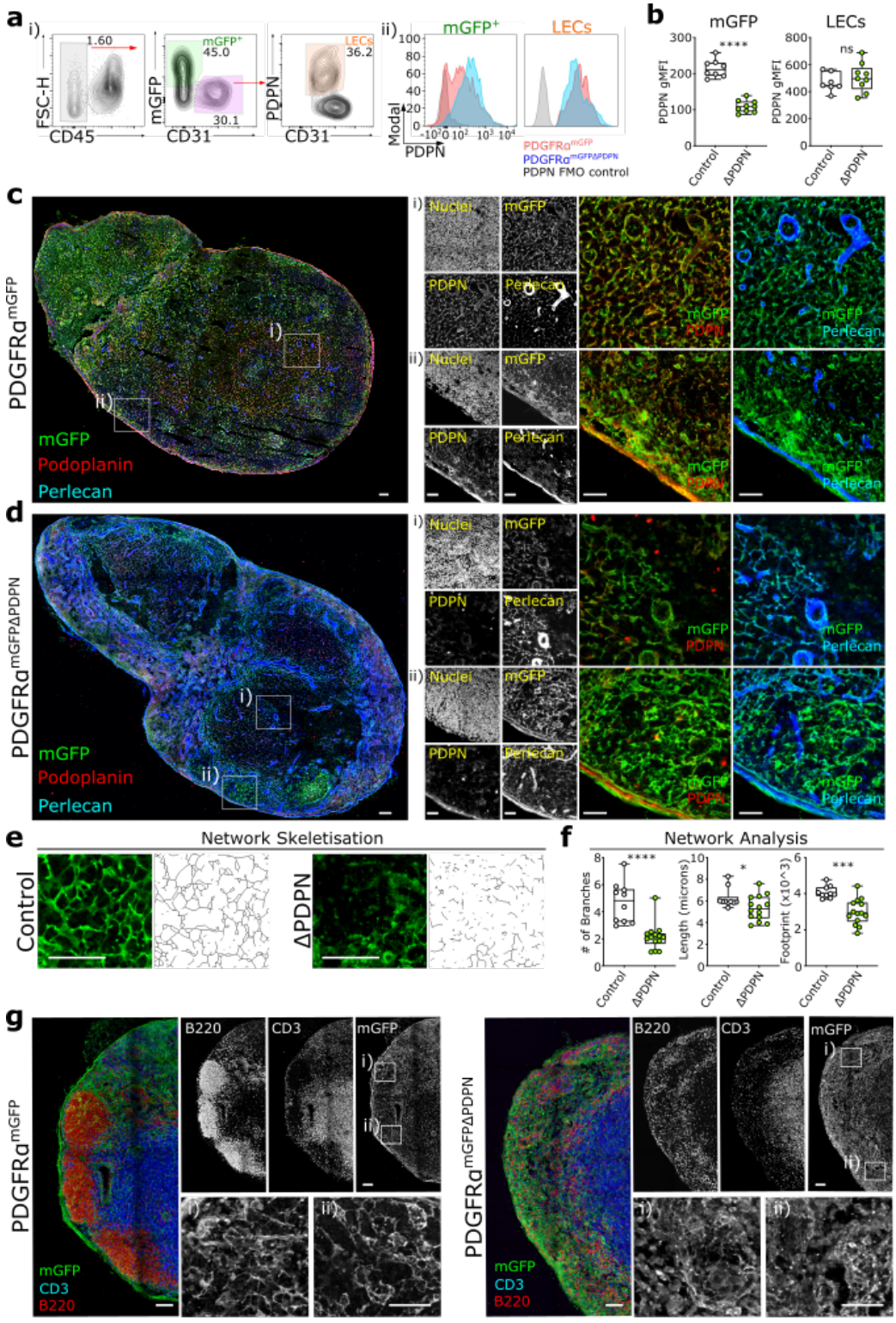

Fig. 7. PDPN^{+} FRCs determine tissue architecture and lymphocyte compartmentalisation PDGFRα^{mGFP} (control) or PDGFR$\alpha^{mGFP\Delta PDPN}$ (ΔPDPN) mice were sacrificed 14-days after tamoxifen treatment. **a,** Flow cytometry gating of (i) GFP^{+} PDGFRα^{mGFP} and lymphatic endothelial cells with (ii) representative histograms of the PDPN expression for each population. **b,** Geometric mean fluorescence intensity (gMFI) of PDPN expression comparing PDGFRmGFP (open circle) and PDGFR$\alpha^{mGFP\Delta PDPN}$ (green circle) previously gated on mGFP+ cells or lymphatic endothelial cells (LEC). N>8 mice for each condition representative of at least 3 independent experiments. Mann-Whitney test (two tailed), ****p<0.0001, ns=no significance. **c,d,** Representative image of lymph node tilescans of PDGFRα^{mGFP} or PDGFR$\alpha^{mGFP\Delta PDPN}$ mice 14 days after tamoxifen treatment c,d, Staining for podoplanin (red), GFP (PDGFRα^{mGFP}, green) and perlecan (blue); zoomed images of **c,d,**(i) paracortex (T cell area) and merged mGFP/PDPN or mGFP/Perlecan; **c,d,**(ii) capsid and merged mGFP/PDPN or mGFP/Perlecan; each showing single channels for DAPI, PDPN, mGFP and Perlecan. **e,** Representative images of FRC network and network skeletisation for PDGFRα^{mGFP} (control) or PDGFR$\alpha^{mGFP\Delta PDPN}$ (ΔPDPN) mice. **f,** Network analysis quantifying the number of network branches, length of branches and network footprint. Network quantification N=10-15 areas of lymph node parenchyma; Mann-Whitney test (two tailed), ****p<0.0001, ***p<0.001, *p<0.05. **g,** Representative image of lymph node tilescans of PDGFRα^{mGFP} or PDGFR$\alpha^{mGFP\Delta PDPN}$ mice 14-days post-tamoxifen treatment staining for mGFP (PDGFRα^{mGFP}; green), CD3 (blue), B220 (red). (i-ii) Selected zooms show the expression of mGFP. Scale bars 50 mum. N>8 mice per condition representative of 3 independent experiments.

sive alterations in gene expression in FRCs. Our findings provide a mechanism for how FRCs can transiently adapt their function through cycles of lymph node expansion to support adaptive immune responses.

PDPN has complex functions which until now have only been partially described. PDPN was first described as a ligand for DC trafficking (28) but has since been shown to also maintain HEV integrity through crosstalk with platelets (50), regulate extracellular matrix deposition (35) and to control the contractility (6, 7) and tissue tension of the FRC network (38). PDPN acts as a mechanical sensor in FRCs to trigger proliferation and lack of PDPN in FRCs attenuates the acute phase of lymph node expansion (38). Now we show that over longer timescales, in steady state, lack of PDPN led to the disruption of the reticular network over time. This phenotype might be partly due to PDPN function as a mechanical sensor on FRCs (38). However, our data additionally reveal that PDPN regulates FRC transcriptional programmes and cell state *in vitro* independently of tissue mechanics. The extensive disruption of the reticular network raises additional questions about a potential role for PDPN in the cell-cell junctions between FRCs. Despite many potential junctional adhesion molecules being identified in both microarray (42) and RNAseq analysis (14), the nature of FRC-FRC cell junctions is still unclear. How PDPN regulates FRC junctions and network connectivity is now to be determined. Interestingly, the extracellular matrix structures of the conduit remained associated with FRCs even when the reticular network was disrupted. We have previously reported that it is the cellular component of the network, the FRCs, that determine the mechanical properties of reticular network (38) – these data would further support that finding since the extracellular matrix scaffolds are seemingly not rigid or strong enough to remain intact once the FRCs detach from their network neighbours.

Fibroblastic stroma is ubiquitous across tissues, yet fibroblasts are specifically adapted to the functional requirements of their microenvironments. Fibroblasts are remarkably plastic, able to change their phenotype and function in response to inflammation or tissue damage (51). Fibroblastic reticular cells of lymph nodes are the archetype 'immunofibroblast' but how fibroblasts in lymphoid tissues differentiate to acquire immunoregulatory functions is not well understood (2, 3). Immunoregulatory fibroblasts can also exist outside of lymphoid tissues. For example, both mouse and human tissue studies indicate that some cancer-associated fibroblasts acquire inflammatory phenotypes and can alter immune function in tumours (51). PDPN^{+} fibroblasts also spontaneously develop in a wide variety of inflammatory conditions (22). Our data confirms the importance of PDPN in the functional phenotype of FRCs, defining additional roles for this glycoprotein ranging beyond regulation of actomyosin contractility and cell mechanics. We now propose that PDPN expression is fundamental to FRC function and may determine 'immunofibroblast' identity.

ACKNOWLEDGEMENTS

This work was supported by a European Research Council Starting Grant (LNEXPANDS; to S.E.A.), a Cancer Research UK Careers Development Fellowship (CRUK-A19763; to S.E.A.), the Medical Research Council (MC-U12266B). We also thank H. Clevers for supplying R26R-confetti mice and S. Watson and C. Buckley for providing the PDPNfl/fl mouse model. We thank the CRUK Centre for Flow Cytometry TTP at UCL Cancer Institute and their staff for support and instrumentation.

Author contributions. S.M. and S.E.A. designed the study and wrote the manuscript. S.M. performed and analysed the majority of experiments. Y.H-G., J.A.C-R., V.G.M., H.L.H. and C.M.d.W. performed RNA-seq analysis. A.C.B. and S.E.A. designed and validated the Pdgfrα-mGFP-CreERT2 mouse model. T.S., R.K. and J.K-V. supported bioinformatics analysis. M.J. performed skeletisation image analysis.

Materials and Methods

Mice. Experiments were performed in accordance with national and institutional guidelines for animal care and approved for the Laboratory for Molecular and Cell Biology by the institutional animal ethics committee review board, European research council, and the UK Home office. Breeding of animal lines were maintained at Charles River Laboratory. For generation of the Pdgfrα-mGFP-CreERT2 and Pdgfrα-mGFP-CreERT2 x Pdpn$^{fl/fl}$ refer to Horsnell et al. 2022. Females and males aged between 8 and 13 weeks were used for experiments, unless stated otherwise.

Tamoxifen administration. Activation of the Cre recombinase was achieved through the administration of tamoxifen (22 mg ml^{1}; Sigma-Aldrich) resuspended in corn oil (Sigma-Aldrich) or sunflower oil (Sigma-Aldrich). Tamoxifen was dosed (82 μg g^{1}) intraperitoneally on 3 consecutive days or by gavage for 5 consecutive days. For immunisation experiments, mice were immunised 7 days after tamoxifen treatment. For steady-state experiments mice were sacrificed 5, 7, 14 and 28 days after tamoxifen treatment. Inguinal and axillary lymph nodes were studied via flow cytometry or confocal microscopy.

Immunization model. *In vivo* immunisations were performed with an emulsion Incomplete Freund's Adjuvant (IFA) or Complete Freund's Adjuvant (CFA) containing SIINFENKL (OVA) (Hooke Laboratories). Mice were injected with 100 μl of the emulsion subcutaneously, 100 μg OVA per mouse, on the right flank at the height of the hip. Animals were sacrificed at 5 and 9 days after immunisations and paired analysis of the inguinal and axillary lymph nodes was performed via flow cytometry and confocal microscopy respectively.

Flow cytometry. Lymph node single cell suspension of 2.5x10^{6} cells was incubated for 20 min at 4^{o}C with a purified rat IgG2b anti-mouse CD16/CD32 receptor antibody (BD biosciences). Cells were stained with fluorochrome-conjugated antibodies against CD9, MAdCAM-1, CD44, CD45, ICAM-1, VCAM-1, CCL21, CD31, PDPN, CD140a, CD62L, CD8a, CD25 , CD3, CD19, CD4 (see Supplementary Table 3 for further Antibody information) for 25 min at 4^{o}C in PBS containing 1% BSA, 5 mM EDTA, 0.05% NaN3. Cells were incubated with fixable viability stain (Supplementary Table 3) for 30 min at 4^{o}C. Cells were fixed and permeabilised using the FOXP3 Fix/perm buffer set (Biolegend) according to the manufacturer's instructions. Cells were permeabilised for 20 minutes at 4^{o}C using the FOXP3 Fix/perm

buffer set (Biolegend) containing purified rat IgG2b anti-mouse CD16/CD32 receptor antibody, followed by staining for Ki-67 and/or FoxP3 (Supplementary Table 3). Samples were analysed on BD LSRFortessa x-50 equipped with 100-mW 405-nm, 100-mW 488-nm, 150-mW 561-nm, 100-mW 637-nm and 60-mW 355-nm lasers with a ND1.0 filter in front of the FSC photodiode. Data was collected on the FACSDiva software (version 7)

Immunofluorescence of tissue sections. Lymph nodes were placed in Antigen fix (DiaPath) and incubated for 2 hours on ice with gentle agitation. Lymph nodes were washed with ice cold PBS and placed in 30% w/v sucrose containing 0.5% NaN3 and incubated at 4°C overnight. The LNs were placed into Tissue-Tek optimum cutting temperature compound and then embedded into moulds containing the optimum cutting temperature compound. Samples were sectioned on the Leica cryostat (CM1950) at a thickness of 15 μm.

For immunofluorescence tissue sections were permeabilised and blocked for 2 hours at room temperature with 10% normal goat serum (NGS), 0.3% Triton X-100 in PBS. Primary antibodies were prepared in the dilutions described in Supplementary Table 3 in PBS containing 10% normal goat serum and 0.01% Triton X-1000 and then centrifuged at 15,000 g for 5 minutes. The antibody cocktail was added to the tissue sections which were incubated overnight at 4°C. Sections were then incubated at room temperature for 1 hour before being washed with PBS-0.05% Tween 20 (3 x 15 minutes at room temperature). Secondary antibodies were prepared similarly to the primary antibodies (dilutions in Supplementtary Table 3) and added to the tissue for 2 hours at room temperature. Sections were then washed with PBS-0.05% Tween 20 (2 x 15 minutes), PBS (1 x 10 minutes) and H_2O (1 x 5 minutes) at room temperature and were then mounted using mowiol mounting media. Images of the tissue were obtained on the Leica TCS SP5 with HCX Plan-Apochromat x40 (NA 1.25) oil lenses. Images were captured at 1,024x1,024 pixels, three-line and 2-frame average onto hybrid pixel or photomultiplier tube detectors. Imaging areas were manually detected, and z-stacks (15-25 μm) were acquired with intervals at 0.3-0.6 μm. Tile scan boundaries were manually set, and images were stitched automatically (numerical, smooth) using the Leica imaging software (LAS AF-2.7.3.9723). Images were analysed on FiJi software (ImageJ).

Network Skeletisation Analysis. Lymph node section fibroblast network was analysed in the parenchymal region of lymph nodes using the Mitochondrial Network Analysis (MiNA) toolset (46). Quantification was performed on ImageJ using the MiNA 3.0.1 macro available on https://gitgub.com/StuartLab/MiNA. Pre-processing of images was set as follows: median filter radius=5, unsharp mask filter radius=10, mask weight=0.6, CLAHE blocksize=127, histogram bins=256 and max slope=3. Data output from MiNA 3.0.1 quantified the mean branch length as the mean length of all lines used to represent the fibroblastic network structures; mean number of network branches the mean number of attached lines used to represent each structure; and the network footprint as the area or volume of the image consumed by the network signal.

Flow cytometry analysis. Flow cytometry data was analysed using FlowJo Software (Tree Star). For tSNE analysis of lymph nodes that were tamoxifen treated, samples were prepared by concatenating 2.5x10^4 $CD45^-$ cells from each condition. The cells were further characterised in two groups to define if they were PDGFRα^{mGFP} or PDGFR$\alpha^{mGFP\Delta PDPN}$. tSNE analysis was performed using the FlowJo package and selecting for the markers: PDPN, CD31, MAdCAM-1, CD9, CD44, ICAM-1, VCAM-1, CCL21 and Ki-67. Clusters were defined manually and confirmed by: back-gating on defined cell populations and comparison the expression of the functional markers used for tSNE analysis. The ViolinPlot package (FlowJo) was utilised to extract the expression of markers by individual cells in each defined cluster. Data was analysed on R Studio and Violin plots comparing the expression of various markers for each defined clustered was performed using the *Geom Split Violin* (*geom_split_violin:Split Violin plot*) function on the *ggplot2* package.

RNA-seq and reads processing. RNA sequencing data from Martinez et al., 2019 are publicly available through University College London's research data repository (doi:10.5522/04/c.4696979).

Differential expression analysis. Differential expression analysis was performed using R 4.0.5 and the DESeq2 package. The gene raw count table (35) was used to calculate differences in transcript expression between samples. As recommended in the package documentation, transcripts with fewer than 10 counts in total were removed from differential expression analysis. In all, 21,285 genes were kept after prefiltering. DESeq2 was used to calculate differences in transcript expression in either PDPN-WT vs PDPN-KO samples, PDPN-WT no CLEC-2 vs CLEC-2 at 6 hours, or PDPN-WT no CLEC-2 vs CLEC-2 at 24 hours (using the contrast function). Differentially expressed genes for each comparison were defined as those with an adjusted p-value smaller than 0.05 and a fold change either log2FC<1.6. (downregulated) or log2FC >1.6 (upregulated). The dplyr package was used for filtering the genes according to their adjusted p-values and fold change. Venn diagrams were plotted using the VennDiagram package. Volcano plots were generated using the ggplot2 package.

Heatmaps. Heatmaps were plotted using TPM (transcript per million) values normalised per gene (Z-score) and clustered using hierarchical clustering using the pheatmap and hclust R packages. Colour palettes were generated using the RColorBrewer package.

Functional annotation analysis. DAVID (52) was for functional annotation. The list of differentially expressed genes (using official gene symbols) was uploaded to the

DAVID website (https://david.ncifcrf.gov/summary.jsp). The table output was then processed using a custom R script. The terms were filtered by fold discovery rate (FDR$\leq$0.05), sorted by fold enrichment and plotted using the dplyr and ggplot2 packages.

Transcription factor analysis. The annotated GO terms were used to identify the transcription factors in the list. Genes were mapped to GO terms using the biomaRt package for R. Transcription factors were then filtered as genes mapped with the GO:0003700 (DNA-binding transcription factor activity) term. Fold change values were plotted using the ggdotchart package.

Functional network analysis. Functional network analysis was carried out using STRING. The lists of differentially expressed genes were submitted to the STRING website (string-db.org/) and analysed using the default values except for the confidence threshold and retaining physical and functional interactions. The confidence threshold was set to the most restrictive value ("very high", 0.9). The networks were then analysed in Cytoscape (53) for visualisation and clustering. Nodes that did not form part of a larger network were hidden (retaining nodes with at least 3 neighbours at level 3). Clustering was performed with the MCODE algorithm (54) using the default parameters. Clusters were manually labelled based on the annotated gene names and descriptions. We filtered the GO terms by statistical relevance and sorted them by fold enrichment (mapped/expected).

YAP/TAZ pathway analysis. Differentially expressed genes were mapped to the Hippo signalling pathway (mmu04390) in the KEGG database. ENSEMBL gene names were used to reduce ambiguity in genes with more than one gene symbol. Output graphics were produced by combining the graphical output from DAVID and the images rendered by the Pathview package for R.

Prism and statistics. Prism9 Software (GraphPad) was used to create graphs and statistical analysis. Comparisons of two data sets was performed using two-tailed Mann-Whitney tests. For comparisons of multiple groups was performed using one- or two-way ANOVA with Tukey's multiple comparison. For all tests, p<0.05 was considered significant.

Bibliography

1. Anne L Fletcher, Sophie E Acton, and Konstantin Knoblich. Lymph node fibroblastic reticular cells in health and disease. *Nature Publishing Group*, 15(6):1 – 12, 05 2015. ISSN 1474-1733. doi: 10.1038/nri3846.
2. Akshay T Krishnamurty and Shannon J Turley. Lymph node stromal cells: cartographers of the immune system. *Nature Immunology*, 21(4):1 – 12, 03 2020. doi: 10.1038/s41590-020-0635-3.
3. Sophie E. Acton, Lucas Onder, Mario Novkovic, Victor G. Martinez, and Burkhard Ludewig. Communication, construction, and fluid control: lymphoid organ fibroblastic reticular cell and conduit networks. *Trends in Immunology*, 42(9):782–794, 08 2021. ISSN 1471-4906. doi: 10.1016/j.it.2021.07.003.
4. Milesa Simic, Iris Manosalva, Lionel Spinelli, Rebecca Gentek, Raheleh R Shayan, Carole Siret, Mathilde Girard-Madoux, Shuaiwei Wang, Lauriane de Fabritus, Janneke Verschoor, Yann M Kerdiles, Marc Bajénoff, Ralf Stumm, Rachel Golub, and Serge A van de Pavert. Distinct Waves from the Hemogenic Endothelium Give Rise to Layered Lymphoid Tissue Inducer Cell Ontogeny. *CellReports*, 32(6):108004, 08 2020. doi: 10.1016/j.celrep.2020.108004.
5. Spyridon Makris, Charlotte M. de Winde, Harry L. Horsnell, Jesús A. Cantoral-Rebordinos, Rachel E. Finlay, and Sophie E. Acton. Immune function and dysfunction are determined by lymphoid tissue efficacy. *Disease Models & Mechanisms*, 15(1):dmm049256, 2022. ISSN 1754-8403. doi: 10.1242/dmm.049256.
6. Sophie E Acton, Aaron J Farrugia, Jillian L Astarita, Diego Mourão-Sá, Robert P Jenkins, Emma Nye, Steven Hooper, Janneke van Blijswijk, Neil C Rogers, Kathryn J Snelgrove, Ian Rosewell, Luis F Moita, Gordon Stamp, Shannon J Turley, Erik Sahai, and Caetano Reis e Sousa. Dendritic cells control fibroblastic reticular network tension and lymph node expansion. *Nature Publishing Group*, 514(7523):498 – 502, 10 2014. ISSN 0028-0836. doi: 10.1038/nature13814.
7. Jillian L Astarita, Viviana Cremasco, Jianxin Fu, Max C Darnell, James R Peck, Janice M Nieves-Bonilla, Kai Song, Yuji Kondo, Matthew C Woodruff, Alvin Gogineni, Lucas Onder, Burkhard Ludewig, Robby M Weimer, Michael C Carroll, David J Mooney, Lijun Xia, and Shannon J Turley. The CLEC-2–podoplanin axis controls the contractility of fibroblastic reticular cells and lymph node microarchitecture. *Nature Immunology*, 16(1):75–84, 01 2015. ISSN 1529-2908. doi: 10.1038/ni.3035.
8. Jean-Philippe Girard, Christine Moussion, and Reinhold Förster. HEVs, lymphatics and homeostatic immune cell trafficking in lymph nodes. *Nature Publishing Group*, pages 1 – 12, 10 2012. doi: 10.1038/nri3298.
9. Cécile Bénézech, Andrea White, Emma Mader, Karine Serre, Sonia Parnell, Klaus Pfeffer, Carl F Ware, Graham Anderson, and Jorge H Caamaño. Ontogeny of Stromal Organizer Cells during Lymph Node Development. *The Journal of Immunology*, 184(8):4521 – 4530, 04 2010. ISSN 0022-1767. doi: 10.4049/jimmunol.0903113.
10. Matthew B Buechler, Rachana N Pradhan, Akshay T Krishnamurty, Christian Cox, Aslihan Karabacak Calviello, Amber W Wang, Yeqing Angela Yang, Lucinda Tam, Roger Caothien, Merone Roose-Girma, Zora Modrusan, Joseph R Arron, Richard Bourgon, Sören Müller, and Shannon J Turley. Cross-tissue organization of the fibroblast lineage. *Nature*, 593(7860):575 – 579, 05 2021. doi: 10.1038/s41586-021-03549-5.
11. Sung Yong Choi, Hosung Bae, Sun-Hye Jeong, Intae Park, Hyunsoo Cho, Seon Pyo Hong, Da-Hye Lee, Choong-kun Lee, Jin-Sung Park, Sang Heon Suh, Jeongwoon Choi, Myung Jin Yang, Jeon Yeob Jang, Lucas Onder, Jeong Hwan Moon, Han-Sin Jeong, Ralf H Adams, Jin-Man Kim, Burkhard Ludewig, Joo-Hye Song, Dae-Sik Lim, and Gou Young Koh. YAP/TAZ direct commitment and maturation of lymph node fibroblastic reticular cells. *Nature Communications*, 11(1):519 – 15, 01 2020. doi: 10.1038/s41467-020-14293-1.
12. Alice E Denton, Edward J Carr, Lukasz P Magiera, Andrew J B Watts, and Douglas T Fearon. Embryonic FAP+ lymphoid tissue organizer cells generate the reticular network of adult lymph nodes. *The Journal of experimental medicine*, 216(10):2242 – 2252, 10 2019. doi: 10.1084/jem.20181705.
13. Isabella Cinti and Alice E Denton. Lymphoid stromal cells—more than just a highway to humoral immunity. *Oxford Open Immunology*, 2(1):iqab011, 2021. ISSN 2633-6960. doi: 10.1093/oxfimm/iqab011.
14. Lauren B Rodda, Erick Lu, Mariko L Bennett, Caroline L Sokol, Xiaoming Wang, Sanjiv A Luther, Ben A Barres, Andrew D Luster, Chun Jimmie Ye, and Jason G Cyster. Single-Cell RNA Sequencing of Lymph Node Stromal Cells Reveals Niche-Associated Heterogeneity. *Immunity*, 48(5):1014 – 1028.e6, 05 2018. doi: 10.1016/j.immuni.2018.04.006.
15. Maria H Ulvmar, Kathrin Werth, Asolina Braun, Poonam Kelay, Elin Hub, Kathrin Eller, Li Chan, Beth Lucas, Igor Novitzky-Basso, Kyoko Nakamura, Thomas Rülicke, Robert J B Nibbs, Tim Worbs, Reinhold Förster, and Antal Rot. The atypical chemokine receptor CCRL1 shapes functional CCL21 gradients in lymph nodes. *Nature Immunology*, 15(7):623 – 630, 05 2014. ISSN 1529-2908. doi: 10.1038/ni.2889.
16. Lutz Menzel, Maria Zschummel, Tadhg Crowley, Vedran Franke, Michael Grau, Carolin Ulbricht, Anja Hauser, Volker Siffrin, Marc Bajénoff, Sophie E. Acton, Altuna Akalin, Georg Lenz, Gerald Willimsky, Uta E. Höpken, and Armin Rehm. Lymphocyte access to lymphoma is impaired by high endothelial venule regression. *Cell Reports*, 37(4):109878, 2021. ISSN 2211-1247. doi: 10.1016/j.celrep.2021.109878.
17. Rémy T. Boscacci, Friederike Pfeiffer, Kathrin Gollmer, Ana Isabel Checa Sevilla, Ana Maria Martin, Silvia Fernandez Soriano, Daniela Natale, Sarah Henrickson, Ulrich H. von Andrian, Yoshinori Fukui, Mario Mellado, Urban Deutsch, Britta Engelhardt, and Jens V. Stein. Comprehensive analysis of lymph node stroma-expressed Ig superfamily members reveals redundant and nonredundant roles for ICAM-1, ICAM-2, and VCAM-1 in lymphocyte homing. *Blood*, 116(6):915–925, 2010. ISSN 0006-4971. doi: 10.1182/blood-2009-11-254334.
18. Viviana Cremasco, Matthew C Woodruff, Lucas Onder, Jovana Cupovic, Janice M Nieves-Bonilla, Frank A Schildberg, Jonathan Chang, Floriana Cremasco, Christopher J Harvey, Kai Wucherpfennig, Burkhard Ludewig, Michael C Carroll, and Shannon J Turley. B cell homeostasis and follicle confines are governed by fibroblastic reticular cells. *Nature Immunology*, 15(10):973 – 981, 08 2014. ISSN 1529-2908. doi: 10.1038/ni.2965.
19. Hsin-Ying Huang, Ana Rivas-Caicedo, François Renevey, Hélène Cannelle, Elisa Peranzoni, Leonardo Scarpellino, Debbie L Hardie, Arnaud Pommier, Karin Schaeuble, Stéphanie Favre, Tobias K Vogt, Fernando Arenzana-Seisdedos, Pascal Schneider, Christopher D Buckley, Emmanuel Donnadieu, and Sanjiv A Luther. Identification of a new subset of lymph node stromal cells involved in regulating plasma cell homeostasis. *Proceedings of the National Academy of Sciences of the United States of America*, 115(29):E6826 – E6835, 07 2018. doi: 10.1073/pnas.1712628115.
20. Cyrille Mionnet, Isabelle Mondor, Audrey Jorquera, Marie Loosveld, Julien Maurizio, Marie-Laure Arcangeli, Nancy H Ruddle, Jonathan Nowak, Michel Aurrand-Lions, Hervé Luche, and Marc Bajénoff. Identification of a New Stromal Cell Type Involved in the Regulation of Inflamed B Cell Follicles. *PLoS Biology*, 11(10):e1001672 – 13, 10 2013. ISSN 1545-7885. doi: 10.1371/journal.pbio.1001672.
21. Miguel Quintanilla, Lucía Montero-Montero, Jaime Renart, and Ester Martín-Villar. Podoplanin in Inflammation and Cancer. *International Journal of Molecular Sciences*, 20(3):707, 2019. ISSN 1422-0067. doi: 10.3390/ijms20030707.
22. Jillian L. Astarita, Sophie E. Acton, and Shannon J. Turley. Podoplanin: emerging functions in development, the immune system, and cancer. *Frontiers in Immunology*, 3:283, 2012. doi: 10.3389/fimmu.2012.00283.
23. K Matsui, S Breiteneder-Geleff, and D Kerjaschki. Epitope-specific antibodies to the 43-kD glomerular membrane protein podoplanin cause proteinuria and rapid flattening of

podocytes. *Journal of the American Society of Nephrology*, 9(11):2013–2026, 1998. ISSN 1046-6673. doi: 10.1681/asn.v9112013.

24. A. Wetterwald, W. Hofstetter, M.G. Cecchini, B. Lanske, C. Wagner, H. Fleisch, and M. Atkinson. Characterization and cloning of the E11 antigen, a marker expressed by Rat Osteoblasts and Osteocytes. *Bone*, 18(2):125–132, 1996. ISSN 8756-3282. doi: 10.1016/8756-3282(95)00457-2.
25. A.K. Rishi, M. Joyce-Brady, J. Fisher, L.G. Dobbs, J. Floros, J. VanderSpek, J.S. Brody, and M.C. Williams. Cloning, Characterization, and Developmental Expression of a Rat Lung Alveolar Type I Cell Gene in Embryonic Endodermal and Neural Derivatives. *Developmental Biology*, 167(1):294–306, 1995. ISSN 0012-1606. doi: 10.1006/dbio.1995.1024.
26. F G Scholl, C Gamallo, S Vilar?o, and M Quintanilla. Identification of PA2.26 antigen as a novel cell-surface mucin-type glycoprotein that induces plasma membrane extensions and increased motility in keratinocytes. *Journal of Cell Science*, 112(24):4601–4613, 1999. ISSN 0021-9533. doi: 10.1242/jcs.112.24.4601.
27. Sirpa Jalkanen and Marko Salmi. Lymphatic endothelial cells of the lymph node. *Nature Reviews Immunology*, 20(9):566 – 578, 09 2020. doi: 10.1038/s41577-020-0281-x.
28. Sophie E. Acton, Jillian L. Astarita, Deepali Malhotra, Veronika Lukacs-Kornek, Bettina Franz, Paul R. Hess, Zoltan Jakus, Michael Kuligowski, Anne L. Fletcher, Kutlu G. Elpek, Angelique Bellemare-Pelletier, Lindsay Sceats, Erika D. Reynoso, Santiago F. Gonzalez, Daniel B. Graham, Jonathan Chang, Anneli Peters, Matthew Woodruff, Young-A. Kim, Wojciech Swat, Takashi Morita, Vijay Kuchroo, Michael C. Carroll, Mark L. Kahn, Kai W. Wucherpfennig, and Shannon J. Turley. Podoplanin-Rich Stromal Networks Induce Dendritic Cell Motility via Activation of the C-type Lectin Receptor CLEC-2. *Immunity*, 37(2): 276–289, 08 2012. ISSN 1074-7613. doi: 10.1016/j.immuni.2012.05.022.
29. Alexander Link, Tobias K Vogt, Stéphanie Favre, Mirjam R Britschgi, Hans Acha-Orbea, Boris Hinz, Jason G Cyster, and Sanjiv A Luther. Fibroblastic reticular cells in lymph nodes regulate the homeostasis of naive T cells. *Nature Immunology*, 8(11):1255 – 1265, 09 2007. ISSN 1529-2908. doi: 10.1038/ni1513.
30. David Oliveira Dias, Hoseok Kim, Daniel Holl, Beata Werne Solnestam, Joakim Lundeberg, Marie Carlén, Christian Göritz, and Jonas Frisén. Reducing Pericyte-Derived Scarring Promotes Recovery after Spinal Cord Injury. *Cell*, 173(1):153–165.e22, 2018. ISSN 0092-8674. doi: 10.1016/j.cell.2018.02.004.
31. Manuel J. Del Rey, Regina Faré, Elena Izquierdo, Alicia Usategui, José L. Rodríguez-Fernández, Abel Suárez-Fueyo, Juan D. Cañete, and José L. Pablos. Clinicopathological Correlations of Podoplanin (gp38) Expression in Rheumatoid Synovium and Its Potential Contribution to Fibroblast Platelet Crosstalk. *PLoS ONE*, 9(6):e99607, 2014. doi: 10.1371/journal.pone.0099607.
32. Harini Krishnan, Julie Rayes, Tomoyuki Miyashita, Genichiro Ishii, Edward P. Retzbach, Stephanie A. Sheehan, Ai Takemoto, Yao-Wen Chang, Kazue Yoneda, Jun Asai, Lasse Jensen, Lushun Chalise, Atsushi Natsume, and Gary S. Goldberg. Podoplanin: An emerging cancer biomarker and therapeutic target. *Cancer Science*, 109(5):1292–1299, 2018. ISSN 1347-9032. doi: 10.1111/cas.13580.
33. Martin Nurmik, Pit Ullmann, Fabien Rodriguez, Serge Haan, and Elisabeth Letellier. In search of definitions: Cancer-associated fibroblasts and their markers. *International Journal of Cancer*, 146(4):895–905, 2020. ISSN 0020-7136. doi: 10.1002/ijc.32193.
34. Lewis S. C. Ward, Lozan Sheriff, Jennifer L. Marshall, Julia E. Manning, Alexander Brill, Gerard B. Nash, and Helen M. McGettrick. Podoplanin regulates the migration of mesenchymal stromal cells and their interaction with platelets. *Journal of Cell Science*, 132(5):jcs222067, 2019. ISSN 0021-9533. doi: 10.1242/jcs.222067.
35. Victor G Martinez, Valeriya Pankova, Lukas Krasny, Tanya Singh, Spyridon Makris, Ian J White, Agnesska C Benjamin, Simone Dertschnig, Harry L Horsnell, Janos Kriston-Vizi, Jemima J Burden, Paul H Huang, Christopher J Tape, and Sophie E Acton. Fibroblastic Reticular Cells Control Conduit Matrix Deposition during Lymph Node Expansion. *CellReports*, 29(9):2810 – 2822.e5, 11 2019. doi: 10.1016/j.celrep.2019.10.103.
36. Ester Martin-Villar, Diego Megias, Susanna Castel, Maria Marta Yurrita, Senen Vilaro, and Miguel Quintanilla. Podoplanin binds ERM proteins to activate RhoA and promote epithelial-mesenchymal transition. *Journal of Cell Science*, 119(21):4541–4553, 2006. ISSN 0021-9533. doi: 10.1242/jcs.03218.
37. Almudena García-Ortiz and Juan Manuel Serrador. ERM Proteins at the Crossroad of Leukocyte Polarization, Migration and Intercellular Adhesion. *International Journal of Molecular Sciences*, 21(4):1502, 2020. doi: 10.3390/ijms21041502.
38. Harry L. Horsnell, Robert J. Tetley, Henry De Belly, Spyridon Makris, Lindsey J. Millward, Agnesska C. Benjamin, Lucas A. Heeringa, Charlotte M. de Winde, Ewa K. Paluch, Yanlan Mao, and Sophie E. Acton. Lymph node homeostasis and adaptation to immune challenge resolved by fibroblast network mechanics. *Nature Immunology*, 23(8):1169–1182, 2022. ISSN 1529-2908. doi: 10.1038/s41590-022-01272-5.
39. Anneli Peters, Lisa A. Pitcher, Jenna M. Sullivan, Meike Mitsdoerffer, Sophie E. Acton, Bettina Franz, Kai Wucherpfennig, Shannon Turley, Michael C. Carroll, Raymond A. Sobel, Estelle Bettelli, and Vijay K. Kuchroo. Th17 Cells Induce Ectopic Lymphoid Follicles in Central Nervous System Tissue Inflammation. *Immunity*, 35(6):986–996, 2011. ISSN 1074-7613. doi: 10.1016/j.immuni.2011.10.015.
40. Pavel Uhrin, Jan Zaujec, Johannes M. Breuss, Damla Olcaydu, Peter Chrenek, Hannes Stockinger, Elke Fuertbauer, Markus Moser, Paula Haiko, Reinhard Fässler, Kari Alitalo, Bernd R. Binder, and Dontscho Kerjaschki. Novel function for blood platelets and podoplanin in developmental separation of blood and lymphatic circulation. *Blood*, 115(19):3997–4005, 2010. ISSN 0006-4971. doi: 10.1182/blood-2009-04-216069.
41. Cécile Bénézech, Saba Nayar, Brenda A. Finney, David R. Withers, Kate Lowe, Guillaume E. Desanti, Clare L. Marriott, Steve P. Watson, Jorge H. Caamaño, Christopher D. Buckley, and Francesca Barone. CLEC-2 is required for development and maintenance of lymph nodes. *Blood*, 123(20):3200–3207, 2014. ISSN 0006-4971. doi: 10.1182/blood-2013-03-489286.
42. Deepali Malhotra, Jillian Astarita, Veronika Lukacs-Kornek, Prakriti Tayalia, Santiago F Gonzalez, Sook Kyung Chang, Konstantin Knoblich, Martin E Hemler, Michael B Brenner, Michael C Carroll, David J Mooney, Shannon J Turley, the Immunological Genome Project Consortium, Yan Zhou, Susan A Shinton, Richard R Hardy, Natalie A Bezman, Joseph C Sun, Charlie C Kim, Lewis L Lanier, Jennifer Miller, Brian Brown, Miriam Merad, Anne L Fletcher, Kutlu G Elpek, Angelique Bellemare-Pelletier, Kavitha Narayan, Katelyn Sylvia, Joonsoo Kang, Roi Gazit, Brian Garrison, Derrick J Rossi, Vladimir Jojic, Daphne Koller, Radu Jianu, David Laidlaw, James Costello, Jim Collins, Nadia Cohen, Patrick Brennan, Michael B Brenner, Tal Shay, Aviv Regev, Francis Kim, Tata Nageswara Rao, Amy Wagers, Emmanuel L Gautier, Claudia Jakubzick, Gwendalyn J Randolph, Paul Monach, Adam J Best, Jamie Knell, Ananda Goldrath, Tracy Heng, Taras Kreslavsky, Michio Painter, Diane Mathis, and Christophe Benoist. Transcriptional profiling of stroma from inflamed and resting lymph nodes defines immunological hallmarks. *Nature Immunology*, 13(5):499, 05 2012. doi: 10.1038/ni.2262.
43. Patricia Severino, Diana Torres Palomino, Heliene Alvarenga, Camila Bononi Almeida, Denise Cunha Pasqualim, Adriano Cury, Paolo Rogério Salvalaggio, Antonio Luiz De Vasconcelos Macedo, Maria Claudina Andrade, Thiago Aloia, Silvio Bromberg, Luiz Vicente Rizzo, Fernanda Agostini Rocha, and Luciana C. Marti. Human Lymph Node-Derived Fibroblastic and Double-Negative Reticular Cells Alter Their Chemokines and Cytokines Expression Profile Following Inflammatory Stimuli. *Frontiers in Immunology*, 8:141, 2017. ISSN 1664-3224. doi: 10.3389/fimmu.2017.00141.
44. Alice A Tomei, Stefanie Siegert, Mirjam R Britschgi, Sanjiv A Luther, and Melody A Swartz. Fluid flow regulates stromal cell organization and CCL21 expression in a tissue-engineered lymph node microenvironment. *Journal of immunology (Baltimore, Md. : 1950)*, 183(7): 4273–83, 2009. ISSN 1550-6606. doi: 10.4049/jimmunol.0900835.
45. Charlotte M. de Winde, Spyridon Makris, Lindsey J. Millward, Jesús A. Cantoral-Rebordinos, Agnesska C. Benjamin, Víctor G. Martínez, and Sophie E. Acton. Fibroblastic reticular cell response to dendritic cells requires coordinated activity of podoplanin, CD44 and CD9. *Journal of Cell Science*, 134(14):jcs258610, 2021. ISSN 0021-9533. doi: 10.1242/jcs.258610.
46. Andrew J. Valente, Lucas A. Maddalena, Ellen L. Robb, Fereshteh Moradi, and Jeffrey A. Stuart. A simple ImageJ macro tool for analyzing mitochondrial network morphology in mammalian cell culture. *Acta Histochemica*, 119(3):315–326, 2017. ISSN 0065-1281. doi: 10.1016/j.acthis.2017.03.001.
47. Jason G Cyster. B cell follicles and antigen encounters of the third kind. *Nature Immunology*, 11(11):989–996, 2010. ISSN 1529-2908. doi: 10.1038/ni.1946.
48. Tina Kwok, Shannon C. Medovich, Ildefonso A. Silva-Junior, Elise M. Brown, Joel C. Haug, Marliece R. Barrios, Karina A. Morris, and Jessica N. Lancaster. Age-Associated Changes to Lymph Node Fibroblastic Reticular Cells. *Frontiers in Aging*, 3:838943, 2022. ISSN 2673-6217. doi: 10.3389/fragi.2022.838943.
49. Basak B. Ural, Daniel P. Caron, Pranay Dogra, Steven B. Wells, Peter A. Szabo, Tomer Granot, Takashi Senda, Maya M. L. Poon, Nora Lam, Puspa Thapa, Yoon Seung Lee, Masaru Kubota, Rei Matsumoto, and Donna L. Farber. Inhaled particulate accumulation with age impairs immune function and architecture in human lung lymph nodes. *Nature Medicine*, pages 1–11, 2022. ISSN 1078-8956. doi: 10.1038/s41591-022-02073-x.
50. Brett H Herzog, Jianxin Fu, Stephen J Wilson, Paul R Hess, Aslihan Sen, J Michael McDaniel, Yanfang Pan, Minjia Sheng, Tadayuki Yago, Robert Silasi-Mansat, Samuel McGee, Frauke May, Bernhard Nieswandt, Andrew J Morris, Florea Lupu, Shaun R Coughlin, Rodger P McEver, Hong Chen, Mark L Kahn, and Lijun Xia. Podoplanin maintains high endothelial venule integrity by interacting with platelet CLEC-2. *Nature*, 502(7469):105 – 109, 10 2013. doi: 10.1038/nature12501.
51. Erik Sahai, Igor Astsaturov, Edna Cukierman, David G DeNardo, Mikala Egeblad, Ronald M Evans, Douglas Fearon, Florian R Greten, Sunil R Hingorani, Tony Hunter, Richard O Hynes, Rakesh K Jain, Tobias Janowitz, Claus Jorgensen, Alec C Kimmelman, Mikhail G Kolonin, Robert G Maki, R Scott Powers, Ellen Puré, Daniel C Ramirez, Ruth Scherz-Shouval, Mara H Sherman, Sheila Stewart, Thea D Tlsty, David A Tuveson, Fiona M Watt, Valerie Weaver, Ashani T Weeraratna, and Zena Werb. A framework for advancing our understanding of cancer-associated fibroblasts. *Nature Reviews Cancer*, 20(3):174 – 186, 03 2020. doi: 10.1038/s41568-019-0238-1.
52. Brad T Sherman, Ming Hao, Ju Qiu, Xiaoli Jiao, Michael W Baseler, H Clifford Lane, Tomozumi Imamichi, and Weizhong Chang. DAVID: a web server for functional enrichment analysis and functional annotation of gene lists (2021 update). *Nucleic Acids Research*, 50 (W1):W216–W221, 2022. ISSN 0305-1048. doi: 10.1093/nar/gkac194.
53. Paul Shannon, Andrew Markiel, Owen Ozier, Nitin S. Baliga, Jonathan T. Wang, Daniel Ramage, Nada Amin, Benno Schwikowski, and Trey Ideker. Cytoscape: A Software Environment for Integrated Models of Biomolecular Interaction Networks. *Genome Research*, 13(11):2498–2504, 2003. ISSN 1088-9051. doi: 10.1101/gr.1239303.
54. Gary D Bader and Christopher WV Hogue. An automated method for finding molecular complexes in large protein interaction networks. *BMC Bioinformatics*, 4(1):2, 2003. ISSN 1471-2105. doi: 10.1186/1471-2105-4-2.

Supplementary Note 1: Supplementary Data

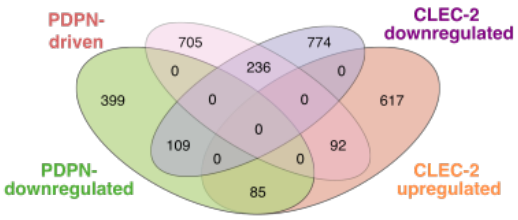

Fig. S1. Control of gene expression by PDPN/CLEC-2 occurs via two independent modes of transcriptional regulation Venn diagram of the differentially genes regulated by PDPN-KD or treatment with CLEC-2 after 6h. This figure supports Fig. 1.

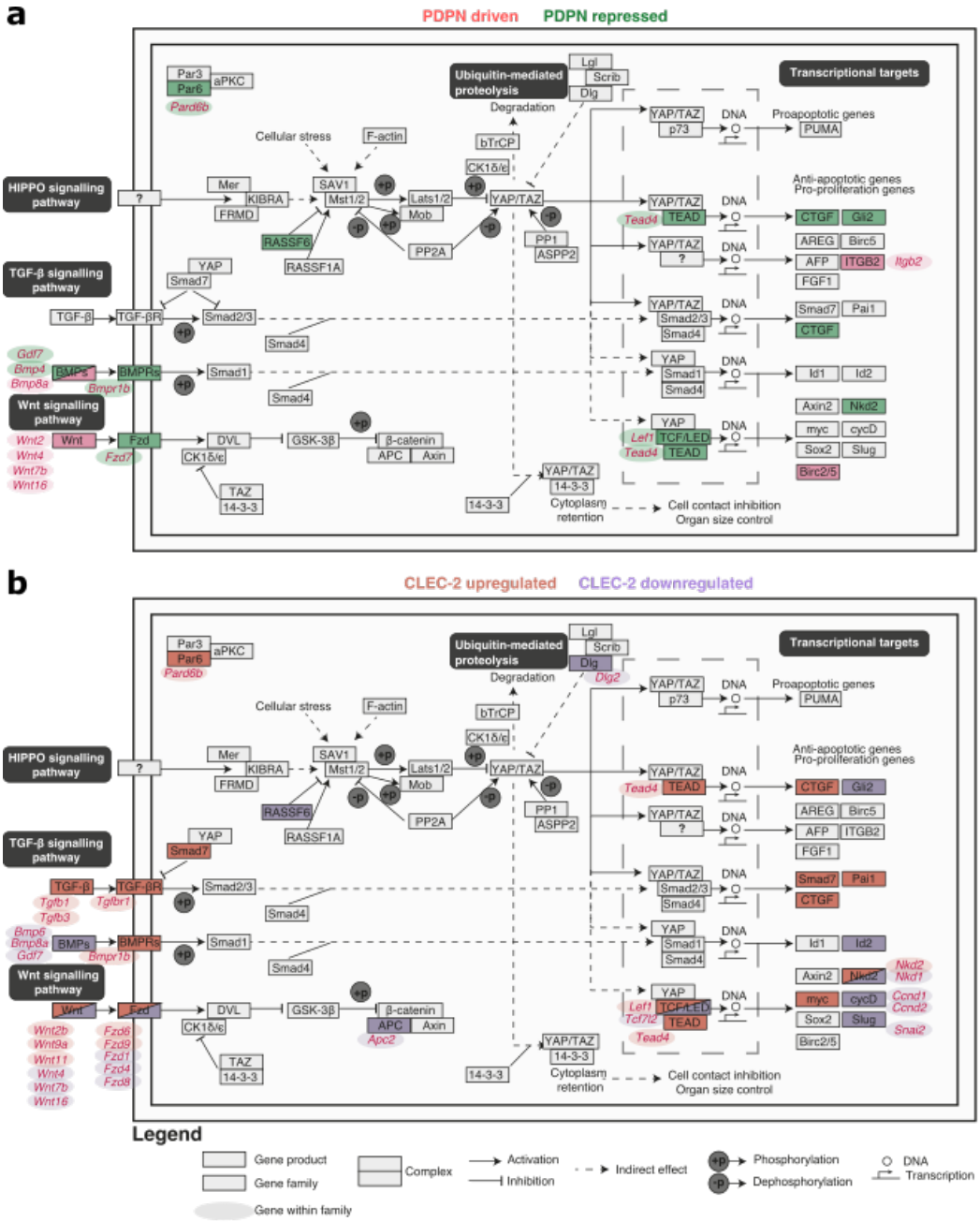

Fig. S2. Transcriptional targets of CLEC-2/PDPN signalling in the YAP/TAZ pathway Genes were mapped to the YAP/TAZ signalling pathway using KEGG. Differentially expressed genes are colour-coded **a,** red for podoplanin driven and green for podoplanin repressed **b,** orange for CLEC-2 upregulated, and purple for CLEC-2 downregulated. Ovals indicate which member within families are regulated. This figure supports Fig. 3.

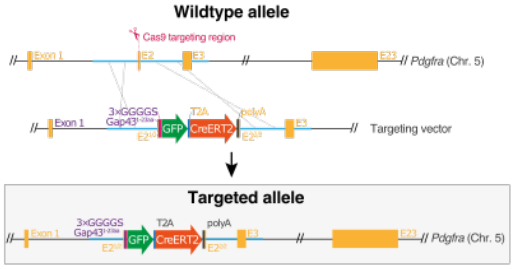

Fig. S3. Conditional deletion of podoplanin in FRCs is replenished Construct for PDGFRα-mGFP-CreERT2 (PDGFRαmGFP) mouse model. This figure supports Fig. 4.

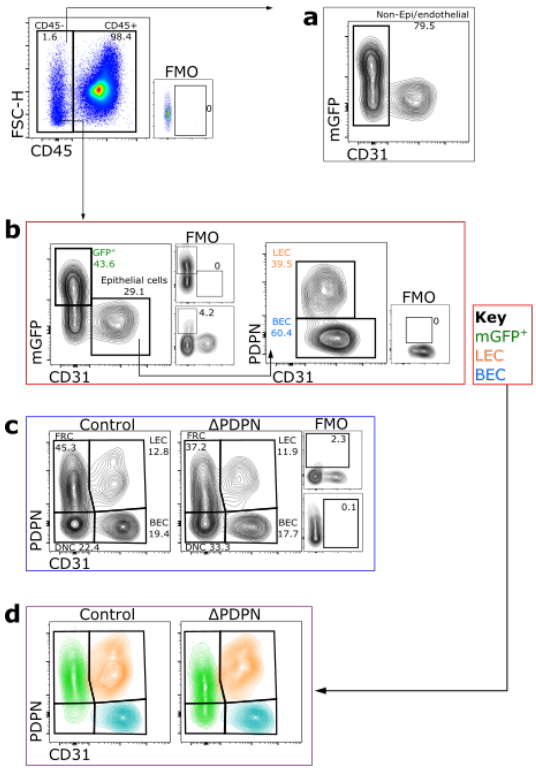

Fig. S4. Stromal cell gating strategy Live, CD45$^-$ (stromal cells) cells where further analysed for stromal cell populations. **a,** Non-epithelial and non-endothelial cells were defined as CD45$^-$CD31$^-$. **b,** GFP$^+$ cells (FRCs) were defined as CD45$^-$CD31$^-$mGFP$^+$; CD31$^+$mGFP$^-$ cells were gated further and lymphatic endothelial cells (LECs) and blood endothelial cells were defined as PDPN$^+$ or PDPN$^-$ respectively. **c,** Conventional gating strategy for FRCs, LECs, BECs and double negative cells (DNCs) which was not used for this analysis as PDPN deletion occurred in FRCs. **d,** Back gating of cell populations from panel b, onto the gating strategy from panel c, to indicate the phenotype of each cell population and comparing control and PDGFR$\alpha^{mGFP\Delta PDPN}$ mice after tamoxifen treatment. Each gate was set based on the fluorescence minus one (FMO) and backgating.This Figure supports Figs. 4-5,7.

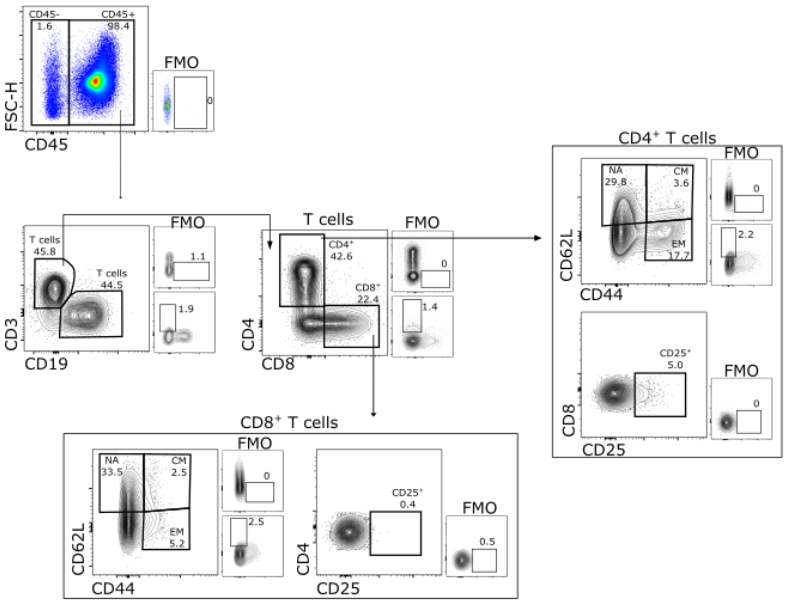

Fig. S5. Adaptive cell gating strategy Live, $CD45^+$ (leukocytes) cells were selected for analysis of adaptive cells. T lymphocytes (T cells) where defined as $CD3^+CD19^-$ and B lymphocytes as $CD3^-CD19^+$. T cells where further gated based on their expression of CD4 or CD8. The activation state of each T cell subset was defined by expression of CD25 or the expression of CD62L and CD44 where cells were defined as: $CD44^+CD62L^-$ (naïve), $CD44^-CD62L^+$ (effector memory) and $CD44^+CD62L^+$ (central memory). Each gate was set based on the fluorescence minus one (FMO) and backgating. This Figure supports Figs. 5.

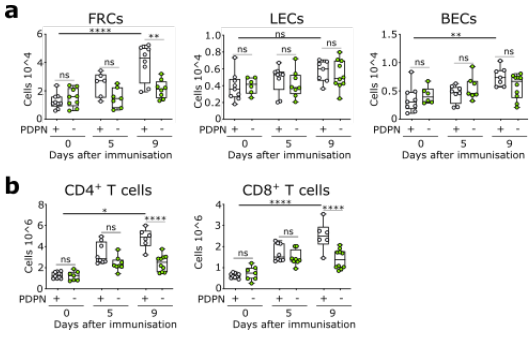

Fig. S6. Number of stromal and T cell populations after immunisation PDGFRα^{mGFP} (open circle) or PDGFR$\alpha^{mGFP\Delta PDPN}$ (green circle) immunised subcutaneously with Incomplete Freund's Adjuvant (IFA) or Complete Freund's Adjuvant (CFA) and ovalbumin 7 days after tamoxifen treatment. **a,** Stromal cell populations were defined as fibroblastic reticular cells (FRCs), lymphatic endothelial cells (LECs) and blood endothelial cells (gating strategy in Figure S4B). **b,** Number $CD4^+$ lymphocytes ($CD4^+$ cells) and $CD8^+$ lymphocytes ($CD8^+$) cells. N=>6 mice, representative of 3 independent experiments. Two-way ANOVA, ****p<0.0001, **p<0.01, *p<0.05, ns=no significance. This Figure supports Figs. 5.

Tables available using the QR code

Table 1. Comparisons of gene expression

Table 2. STRING analysis

Table 3. Flow cytometry and Microscopy antibodies and reagents